CYSTEINE AND SPIN LABEL MODIFICATION AS A MEANS TO EXPLORE PROTEIN DYNAMICS AND STRUCTURE

By

Marshall Scott McGoff

B.S. in Chemistry, Worcester Polytechnic Institute, 2008

Submitted to the Graduate Faculty of Kenneth P.

Dietrich School of Arts and Sciences in partial fulfillment

of the requirements for the degree of

Master of Science

University of Pittsburgh

2012

UNIVERSITY OF PITTSBURGH

DIETRICH SCHOOL OF ARTS AND SCIENCES

This thesis was presented

By

Marshall Scott McGoff

It was defended on

November 19, 2012

and approved by

Dr. W. Seth Horne, Assistant Professor, Department of Chemistry

Dr. Sean Garrett-Roe, Assistant Professor, Department of Chemistry

Thesis Adviser: Dr. Sunil Saxena, Associate Professor, Department of Chemistry

CYSTEINE AND SPIN LABEL MODIFICATION AS A MEANS TO EXPLORE PROTEIN DYNAMICS AND STRUCTURE

Marshall Scott McGoff, M.S.

University of Pittsburgh, 2012

The goal of this work is to expand upon the current labeling technology available in the field of site directed spin labeling (SDSL) by cysteine and spin label modification. Multiple mutants of the B1 immunoglobulin-binding domain of protein G (GB1) were expressed, purified, characterized, and described herein. The synthesis and full characterization is described for several initial compounds along the pathway to a more rigid linker with less orientational freedom. The modification of cysteine using O-mesitylenesulfonylhydroxylamine (MSH) to form dehydroalanine with subsequent attachment of a thiol is detailed in this work. Electron Spin Resonance (ESR) spectra were collected as a means for comparison to newly designed labels. Future directions for the project include the completion of the synthesis and incorporation of new spin labels using dehydroalanine.

TABLE OF CONTENTS

LIST OF FIGURES

1.0. INTRODUCTION

The focus of this work is to expand upon currently available labeling techniques and labels in the field of site directed spin labeling (SDSL) with regards to electron spin resonance (ESR). SDSL is a powerful technique that allows the determination of the dynamics and structure within a biological system. Currently, the most widely used and well-studied spin label is MTSSL (Figure 1), which attaches to a free cysteine by creating a disulfide linkage with 5 dihedral angles of rotation. The dynamics of the spin label are determined by analyzing the lineshape from the continuous wave (CW) experiment in conjunction with modeling and simulations. Another ESR experiment called double electron electron resonance (DEER) can be used to generate distance distributions between two spin labels in a system. However, both of these experiments are sensitive to the fluctuations in the backbone as well as the dynamics of the label itself, which necessitates the use of complex modeling to understand the spectra.

A rigid spin label with lower orientational freedom will have fewer possible orientations available and therefore will be less complex to model, which is a major goal. To this end, the synthesis of a new spin label is discussed with fewer rotatable bonds between the protein backbone and the ring containing the nitroxide. This work will show the initial compounds towards this goal including the synthesis and fully characterization with ^{1}HNMR, ^{13}CNMR, and

high resolution mass spectrometry. In addition, the future steps in the pathway are mapped out to the desired piperidine based spin label.

This work will focus on a reagent known as O-mesitylenesulfonylhydroxlamine (MSH) that has been shown to convert cysteines to dehydroalanine in a solvent exposed loop region of a protein. This work utilizes the B1 immunoglobulin-binding domain of protein G (GB1) and will show that the conversion to dehydroalanine and the subsequent attachment of a thiol works in the model protein system in a loop region.

2.0. BACKGROUND

2.1. SITE DIRECTED SPIN LABELING

Site directed spin labeling (SDSL) has emerged as a powerful tool for using electron spin resonance (ESR) [1-7] and nuclear magnetic resonance (NMR) [8-11] spectroscopy to observe protein dynamics and structure. SDSL initially involves the mutation of specific residues under examination to cysteines using site directed mutagenesis (SDM). The use of cysteine in SDSL is twofold; it is the only natural amino acid that contains a free thiol, and it is not commonly found in a protein unless it is involved in the structure or function.

Disulfide bonds can play a role in the folding process as well as increasing the folded stability of a protein [12-14]. Cysteines can also be vital to the function of a protein in the form of a metal binding site or an iron-sulfur cluster [15, 16]. Once the cysteines in a protein have been determined to not be functionally or structurally important, they can be mutated to alanines to avoid being labeled erroneously. After removing all non-essential cysteines, the residues of interest can be mutated to cysteines in order to be labeled using SDM. The ability to selectively change a residue of interest into a cysteine and then spin label for ESR measurements is a

powerful tool. This technique allows researchers to explore a specific area of the protein or an entire region by mutating the region residue by residue.

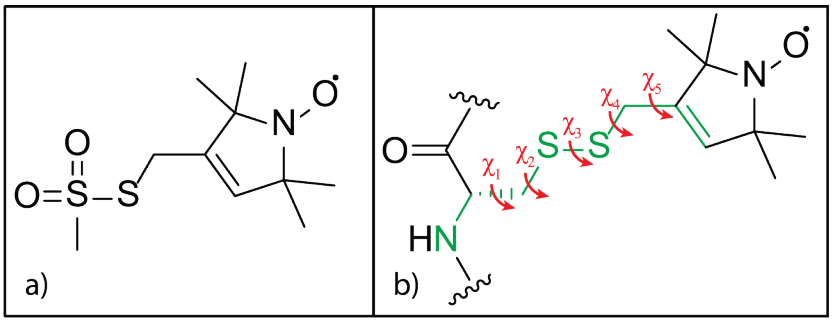

Figure 1: MTSSL (a) and R1 (b)

The current trend involves the use of a flexible nitroxide linker known as methanethiosulfonate spin label (MTSSL, Figure 1a), which is a sulfhydryl specific reagent that creates a disulfide bond with free thiols such as cysteine. One of the disadvantages of this label is the inherent flexibility of the linker. R1 has 5 rotatable bonds with dihedral angles between the linker attachment and the nitroxide ring denoted as χ_1 to χ_5 (Figure 1b), which can make the deconvolution of protein dynamics from spin label dynamics difficult. Through crystallization [17-19] and computational modeling [20, 21], various preferred orientations of these angles have been determined for surface exposed alpha helical sites. One important finding from these studies was the existence of a hydrogen bond between the H_α and the S_δ which is theorized to limit the rotational freedom of the first two bonds [22]. The rotation about the disulfide bond (χ_3) has been known to be slow on the ESR timescale and therefore most of the flexibility in R1 is due to the last two dihedral angles (this theory is known collectively as the χ_4/χ_5 model since the flexibility in the label comes from χ_4/χ_5 [20]). The observation that the hydrogen bond between the H_α and the S_δ can be useful to "tether" the spin label and reduce the dynamics about the first 3 chi angles in MTSSL is

important and will be used as a point of comparison in future studies with structurally different spin labels. Therefore, the hydrogen bond is thought to be stabilizing and important in limiting the mobility of MTSSL.

While this theory is well supported by examples in alpha helices, whether in solvent exposed, buried or membrane sites, there is little work done in other secondary structure environments. Recent work by our group on beta-sheets (solvent-exposed on an interior strand of a twisted beta-sheet) has shown that conformations of the R1 side chain that do not have a hydrogen bond between the H_α and the S_δ can exist in a beta-sheet environment [18]. It was determined using variable temperature CW studies that there are two different components in the CW spectra: a mobile component that dominates at higher temperatures, and a more immobile component that is likely due to the formation of a hydrogen bond. Using the crystal structure obtained for the doubly labeled sample, it was geometrically impossible for one of the rotamers to have a hydrogen bond. Therefore, the rotamer lacking the hydrogen bond was assigned to be the more mobile component.

Other recent work [23] on a beta sheet environment in cellular retinol binding protein (CRBP) made similar observations in regards to possible hydrogen bond formation between the H_α and the $S_{\delta.}$ The predictions in the paper, since there are no associated crystal structures, strongly coincide with those of our work. This highlights the importance of the hydrogen bond in reinforcing the ordered environment desired for ESR measurements of the local environment.

Interestingly, a label that cannot form the hydrogen bond in question has been developed (Figure 2a) [24]. This label (known as R3 when bound to a protein, Figure 2b), contains a halogen that will react with the thiol of a cysteine and form a thioether bond. Since there is no S_δ, the hydrogen bond is noticeably absent. It was also noted that R3 was more mobile than R1 in an alpha helix (the mobility was determined by the peak-to-peak first derivative width of the central spectral peak). Also troubling was that this label resulted in nonspecific labeling and a strong background signal.

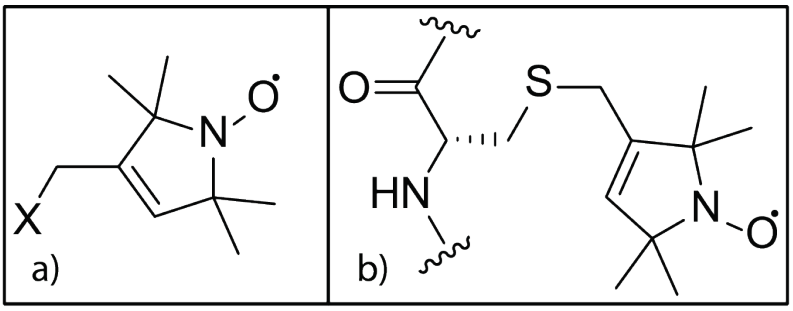

Figure 2: Spin label with halogen leaving group (a) and R3 (b)

While important, this work brings up several problems in the area of spin labeling. First, most work focuses on alpha helices as the secondary structure of choice, which makes modeling comparisons difficult in other environments. Secondly, the use of an alkyl halide to introduce a more stable thioether bond is not a desireable pathway due to nonspecific labeling. A novel approach is needed for the nonspecific incorporation of a thioether bond by which to attach a spin label. An important point to keep in mind is that the hydrogen bond is thought to be

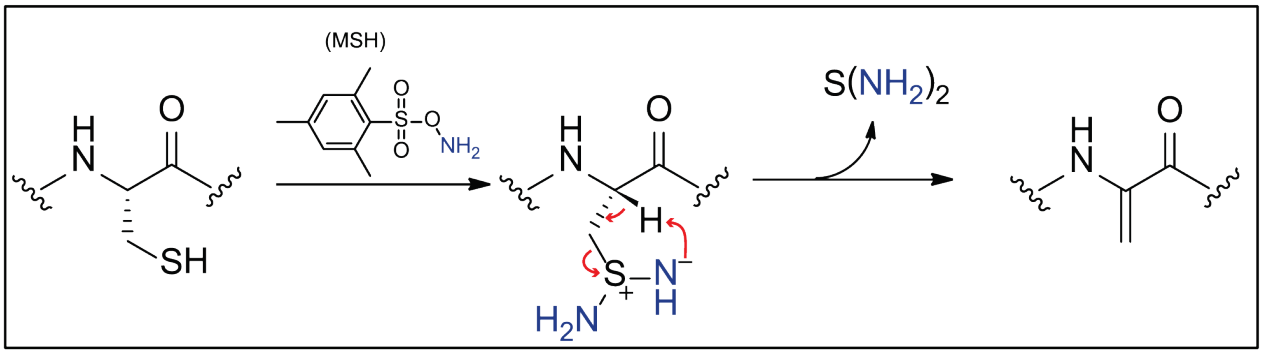

Figure 3: Mechanism for MSH conversion of cysteine (left) to dehydroalanine (right)

stabilizing and little work has been done on spin labels that do not contain it.

A route expanding upon the work of a 2008 paper [25] is to be explored here. In this paper, the authors describe a reagent to selectively modify existing cysteines to an alkene side chain referred to as dehydroalanine (Figure 3, right). This reagent is known as O-mesitylenesulfonylhydroxylamine (MSH) and works by an oxidative elimination mechanism (Figure 3, middle). The author expands upon this research and illustrates several different pathways to get to this product [26]. Once the alkene was obtained using any of the methods, it was then shown that thiols were highly reactive towards this new functionality. Using this approach with a thiol containing spin label, the end result could resemble that of R3 with only one sulfur atom involved in connecting the nitroxide ring to the protein.

One advantage to using a label such as R3 is that there will be less rotatable bonds between the C_α and the radical. Not only are there less rotatable bonds but the length of the linker is one bond shorter. The idea is that with a shorter linker, the motion of the nitroxide will be more directly related to the motion of the backbone. Especially with distance measurements in mind, the shorter the linker the more accurate the distance being measured is. Ideally the goal is to incorporate a very rigid linker such as TOAC (2,2,6,6-tetramethyl-N-oxyl-4-amino-4-carboxylic acid, Figure 4) that does not interfere with the backbone motion or the folding of the protein itself. TOAC has been used in peptide synthesis as a rigid spin label for ESR studies but there are several problems with its use [27]. The main issue is that the spin label must be engineered into the protein using peptide

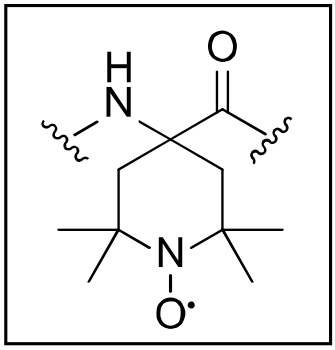

Figure 4: The amino acid spin label TOAC

synthesis [28]. Unfortunately there are limitations with peptide synthesis related to the size of the protein being synthesized and therefore TOAC would be impossible to incorporate into large protein systems.

By utilizing dehydroalanine and the linker chemistry available, a free thiol could be used to create a thioester instead of a disulfide with traditional labeling. By using a free thiol, a shorter spin label could be attached via a Michael addition. The alkene in dehydroalanine is electrophilic and will act as a Michael acceptor with a strong nucleophile such as a thiol being the Michael donor [29]. One possible problem with this approach is that the starting alkene is achiral and upon reaction becomes a chiral center with two possible isomers. Fortunately there is evidence in the literature of ways to make this reaction stereospecific [30]. It is possible that the chiral environment of the protein system will only allow one stereoisomer for the reaction. After attaching a thiol to the protein, it will be important to determine the absolute configuration within the system in order to understand the usefulness of this reaction scheme. X-ray crystallography would be the easiest way to assign absolute configuration but it would also be possible using 2D NMR [31].

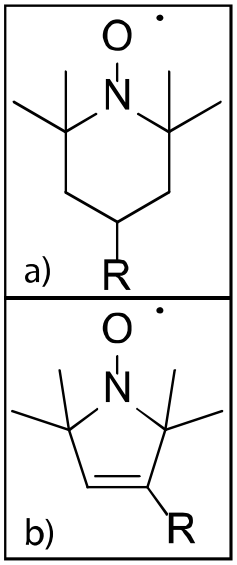

Figure 5: Representative piperidine (a) and pyrroline (b) nitroxides

After analyzing the linker and attachment scheme, attention must be paid to the structure of the ring containing the nitroxide. There are several variables to consider including ring size, substituents, and structure. For example, MTSSL is a tetramethyl substituted pyrroline (Figure 5b) which is the most commonly used nitroxide ring size. There has been much less

work utilizing substituted piperidine rings (Figure 5a). The advantage to using a 6 membered ring is that the ring will adopt a chair configuration due to the stability imparted by this conformation. The methyl substitutions are important to provide steric hindrance to prevent the reduction of the radical [32]. Therefore, any modifications to the nitroxide ring structure will include the tetramethyl substituents or an equivalent alkyl chain. MTSSL also contains a double bond within the ring but there are several analogs that do not.

2.2. ESR TECHNIQUES – CONTINUOUS WAVE (CW)

Once a spin label has been attached to the protein of interest, ESR experiments can be performed to gather information about the system. There are two main types of experiments in ESR, CW and pulse, which both provide different types of information. CW-ESR couples unpaired electrons in a magnetic field (denoted B_0) with the application of microwave radiation (v). Initially there are several quantum mechanical energy levels that correspond to the possible states that the particle (electron in this case) can exist in. For an electron, there are two states, which correspond to the spin state of the electron, that are degenerate in energy under normal circumstances. However, after the application of the magnetic field, the degeneracy in these energy levels is lifted creating an energy separation between the two. When the energy of the microwave radiation is equal to the difference in energy between these two levels, absorption occurs and is indicated by a difference in the detector current [33]. Instrumentally, we have to

scan the magnetic field while keeping the frequency of the microwave constant. Since the magnet is typically an electromagnet, the magnetic field strength can be controlled by the amount of current being applied and thus be tuned very precisely.

In order to understand why absorption occurs in the first place, it would be helpful to understand the quantum mechanical background information. Firstly, the spin labels that we will be focusing on contain nitroxide radicals, which have a free electron. An electron, being an intrinsic spin ½ particle, has two initially degenerate energy levels which are separated with the application of the magnetic field. The interaction of the electron with the magnetic field is known as the Electron Zeeman Interaction. For a free electron, the Hamiltonian associated with the interaction is:

$$\hat{H}_{EZ} = g_e \beta_e \vec{B} \cdot \hat{S}$$

where g_e is the g-factor for a free electron, β_e is the Bohr magneton for an electron, $\hat{S}$ is the spin angular momentum operator. The spin angular momentum operator ($\hat{S}_z$) is a quantum mechanical operator that operates on the spin wavefunction of the electron. The z-direction is used because of the convention for the applied magnetic field (B) to be in the z-direction. The wavefunction of the electron, with a spin (S) of ½, has two states with m_s values of ±½. M_s is the observable value for our operator and has 2S + 1 values that range from -s to s increasing by 1 (-s, -s+1 … s-1, s). For an electron, it means there are two m_s values of –½ and +½. Often $\vec{B}$ is shown as B_0 because of the convention for the z-direction to be the direction of the applied magnetic field:

$$\vec{B} = (0 \;\; 0 \;\; 1) = B_0$$

Therefore the energies for the two different energy levels for the electron are:

$$E = g_e \beta_e B_0 m_S = \pm \frac{1}{2} g_e \beta_e B_0$$

The g-factor is related to the magnetic moment and gyromagnetic ratio of the electron and varies depending on the local environment. The resonance equation for the transition of a free electron in a vacuum is governed by the equation:

$$hv = g_e \beta_e B_0$$

where g_e is the g-factor for a free electron in a vacuum and is well known to extraordinary certainty (2.002319) [34]. The value of g in a real system is different because of the local environment of the electron. As the electron orbits the nucleus about a magnetic field, it produces a secondary magnetic field ($B_{induced}$) which will affect the local magnetic field. In order to take this effect into account, we can rearrange the initial equation to the following:

$$hv = g_e \beta_e (B_0 + B_{induced})$$

Since it will be technically very difficult to measure the value of $B_{induced}$ directly, we can consider it to be some factor of B_0 ($B_{induced} = nB_0$). We use nB_0 because we cannot directly measure the change in B but know that it is some factor of B_0. We then substitute and simplify the equation to this:

$$hv = g_e \beta_e B_0 (1 + n)$$

We can now rearrange to the final equation:

$$hv = g \beta_e B_0$$

where $g = g_e(1 + n)$ and is a measurable quantity in our ESR measurements. It is similar to chemical shift (δ) in NMR and provides information about the electronic structure of the molecule. The g value also changes based on the shape of the orbital that it is delocalized into. At room temperature g is an isotropic value because the spin label is tumbling too quickly to detect changes in orientation. Therefore all of the possible orientations are averaged out to a single isotopic value for g. When the temperature is lowered, g become a 3x3 tensor with diagonalized values of g_{xx}, g_{yy}, and g_{zz} which are the values for g when B_0 is aligned along the x, y, and z directions respectively.

For nitroxides, the radicals are delocalized around the nitrogen – oxygen bond. The interaction of the nuclei in the magnetic field is known as the Nuclear Zeeman Effect, which is analogous to the Electron Zeeman. Since the radical is delocalized around the nitrogen-oxygen, the properties of the nitrogen and oxygen nuclei become important. Oxygen-16 has a nuclear spin of 0 meaning that it will not have an interaction with the magnetic field. However, Nitrogen-14 has a nuclear spin (I) of 1 giving it three states from the 2I +1 rule with values (m_I) of -1, 0, and 1. With this information, the energy of the nuclear Zeeman can be written as:

$$E = -g_n \beta_n B_0 m_I$$

The next interaction is between the nuclei and the electron which is referred to as the hyperfine interaction (A). The energy of this interaction can be broken down into two types of interactions known as the Fermi contact and Dipolar Coupling. The Hamiltonian for the hyperfine is a combination of both of these interactions:

$$\hat{H}_{Hyp} = \hat{H}_{FC} + \hat{H}_{DC}$$

The Fermi contact is the interaction between the magnetic moments of an electron and nuclei when the electron is at that nucleus. This interaction only occurs with s-orbitals since only they have non-zero electron density at the nucleus. Since there is no orientationally selective term such as an angle, the hyperfine splitting related to the Fermi contact is observable at room temperature. The Hamiltonian that describes the Fermi contact can be described as:

$$\hat{H}_{FC} = \hat{S} \cdot \vec{\vec{A}} \cdot \hat{I}$$

Dipolar coupling is a long distance interaction between the magnetic moments of the electron and nuclei. The dipolar coupling an orientationally dependent term but at room temperature the global tumbling of the molecule is too fast for the ESR timescale. Therefore all of the orientations are averaged out and the term goes to zero at room temperature. When the temperature is lowered, similar to the case of the g factor, A becomes a 3x3 tensor with diagonal values of A_{xx}, A_{yy}, and A_{zz} which are the values for A when B_0 is aligned along the x, y, and z axis respectively. The Hamiltonian for the dipolar coupling is:

$$\hat{H}_{DC} = \frac{\hat{\mu}_S \cdot \hat{\mu}_I}{r^3} - \frac{3\langle \hat{\mu}_S \cdot \vec{r} \rangle \langle \hat{\mu}_I \cdot \vec{r} \rangle}{r^5}$$

where $\vec{r}$ is the vector that connects the electron and nuclear magnetic moments. The most important part of this equation is the r^3 dependence on the coupling. Using all of this information, the complete room temperature Hamiltonian can be constructed and is shown as Figure 6:

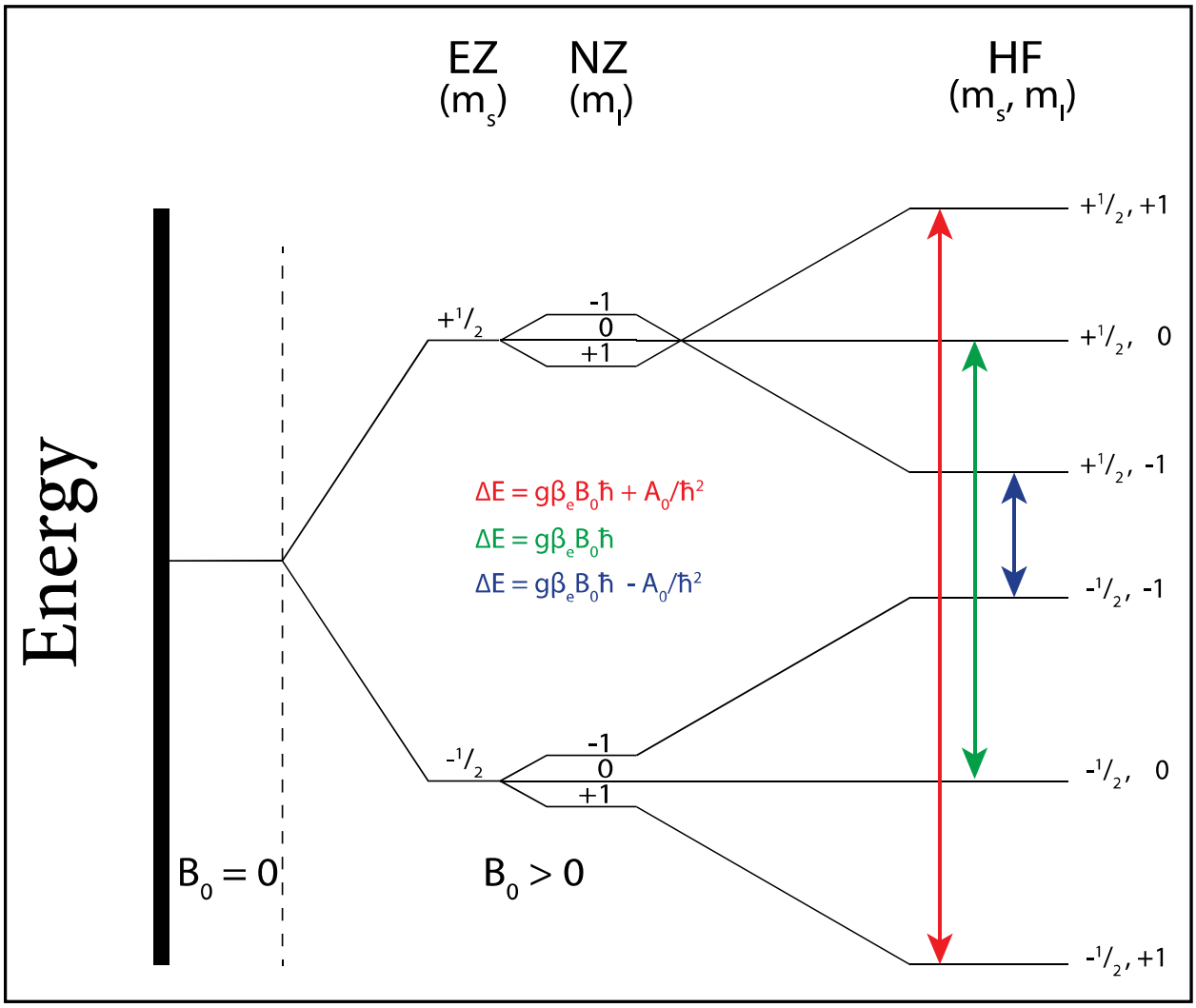

Figure 6: Nitroxide Energy Manifold

$$\hat{H} = \hat{H}_{EZ} + \hat{H}_{NZ} + \hat{H}_{Hyp}$$

$$H = g\beta_e B_0 \hat{S}_z - g_n \beta_n B_0 \hat{I}_z + A_0 \hat{S}_z \cdot \hat{I}_z$$

$$E = g\beta_e B_0 m_S \hbar - g_n \beta_n B_0 m_I \hbar + \frac{A_0}{\hbar^2} m_S m_I$$

$$\Delta E = g\beta_e B_0 \hbar + \frac{A_0}{\hbar^2} m_I$$

According to the 2I+1 rule and the ESR selection rules ($\Delta m_S = \pm 1$, $\Delta m_I = 0$), there should be 3 different transitions. The energy of each transition is given in the final equation as ΔE. The nuclear Zeeman is noticeably absent as it cancels out in the difference in the energy levels. At room temperature then the expected spectrum would have 3 peaks with equal intensities. In actuality the spectrum is very different with major deformation in the $m_I = \pm 1$ transitions. A sample spectrum for MTSSL bound to a protein (denoted R1 when bound) is shown in Figure 7.

There are several reasons why the actual spectrum differs from the theoretical spectrum and can be explained by the motion of the spin label itself. After the nitroxide binds to a protein, the rotational correlation time for the label increases as the size of the protein increases. Once the nitroxide is bound, it will become sensitive to the fluctuations in the motion of the protein. If the label itself is very disordered or mobile, changes in the protein will be less noticeable. As the label becomes more ordered or rigid, it will become more sensitive to the backbone motions of the protein system it is attached to.

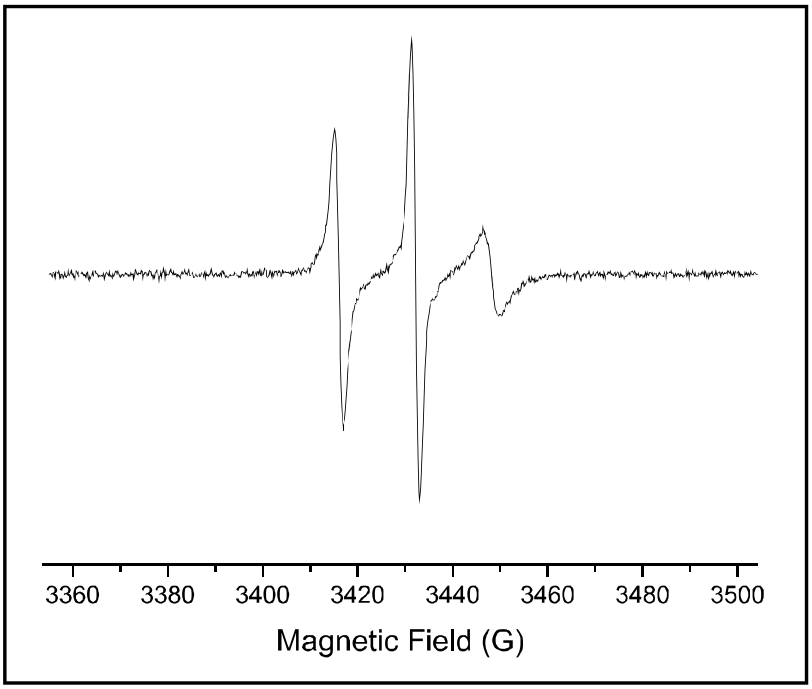

Figure 7: Room temperature CW-ESR for R1

In this work, we will be using an X-band spectrometer (~9.5 GHz). Molecular tumbling of a small protein, for example a 6kDa protein, at room temperature is typically on the order of ~10^{-10} seconds while the X-band ESR timescale is 10^{-9}, which will average all of the possible orientations of the spin label in the system. A viscous buffer solution such as 30% Ficoll 70 can be used to slow down the rotational correlation time of global tumbling of that protein so that it does not substantially contribute to ESR lineshape. The viscosity (η) of water is ~1 mPa*s whereas a 30% w/v Ficoll 70 solution would have an η = 4.8 mPa*s [35].

Once the spectrum has been obtained, the mobility of the spin label at each location can be fit at variable temperatures using modeling. In particular, a model known as the microscopic order macroscopic disorder (MOMD) can be utilized to extract parameters such as the rotational correlation time of the spin label (τ) [36]. This value is inversely related to the mobility at the associated site meaning a lower value is indicative of a more mobile spin label. Another important value is S_{20}, known as the order parameter, which reflects the decrease in mobility of the spin label due to the backbone and is commonly attributed to the hydrogen bond between H_α and S_δ [37, 38]. Therefore, by using site-directed mutagenesis on several locations and using the same spin label, the mobility of the several sites can be determined. Equivalently, by using several different spin labels on the same site, the mobility of each spin label can be directly compared.

2.3. ESR TECHNIQUES – DOUBLE ELECTRON ELECTRON RESONANCE (DEER)

Before delving into any specific pulse sequence, it will be important to understand how pulsed-ESR works in general. Similar to CW-ESR, microwave radiation is applied to the sample but in pulse experiments, the microwave radiation is in short, strong bursts. Initially the spins are precessing about the magnetic field (B_0) which is in the z-direction by convention. When a pulse is applied, it will tip the spins from the z-direction based on the strength of the pulse. The strength of the pulse is inversely related to the length of the pulse so short pulses will tip the spins more strongly. Pulses are often abbreviated by their tip angle to make it clearer what the strength of the pulse is. The most commonly used pulses are π and $\pi/2$ which tip the spins 180° and 90° respectively.

A simple pulse sequence is the generation of a Hahn echo which involves π and $\pi/2$ pulses [39]. The $\pi/2$ pulse first reorients the spins into the x-y plane where the spins start to fan out along the plane. This fanning out happens because of several different off resonance precessional frequencies in the spin system due to minor differences in the local magnetic field from an inhomogeneous magnetic field across the entire sample. The π pulse then flips the spins 180° which causes the spins to precess in the opposite direction. Since some of the spins are precessing at different rates, the reversal of the precession will continue in the opposite direction causing the spins to "refocus" into what is known as an "electron spin echo" (ESE). The time between the pulses can be stepped out and the echo intensity as a function of the separation between the pulses to determine the relaxation rate of the system. The relaxation

time is the time that it takes for the applied net magnetization to decay. There are several processes that are involved in relaxation with the two main sources being spin-lattice (T_1) and spin-spin relaxation (T_2). With this information in mind, the pulsed experiment that will be utilized in this work is the DEER experiment.

The pulsed ESR experiment DEER can be used to generate a distance distribution between two paramagnetic centers between 2-8 nm by measuring the dipolar coupling between the two

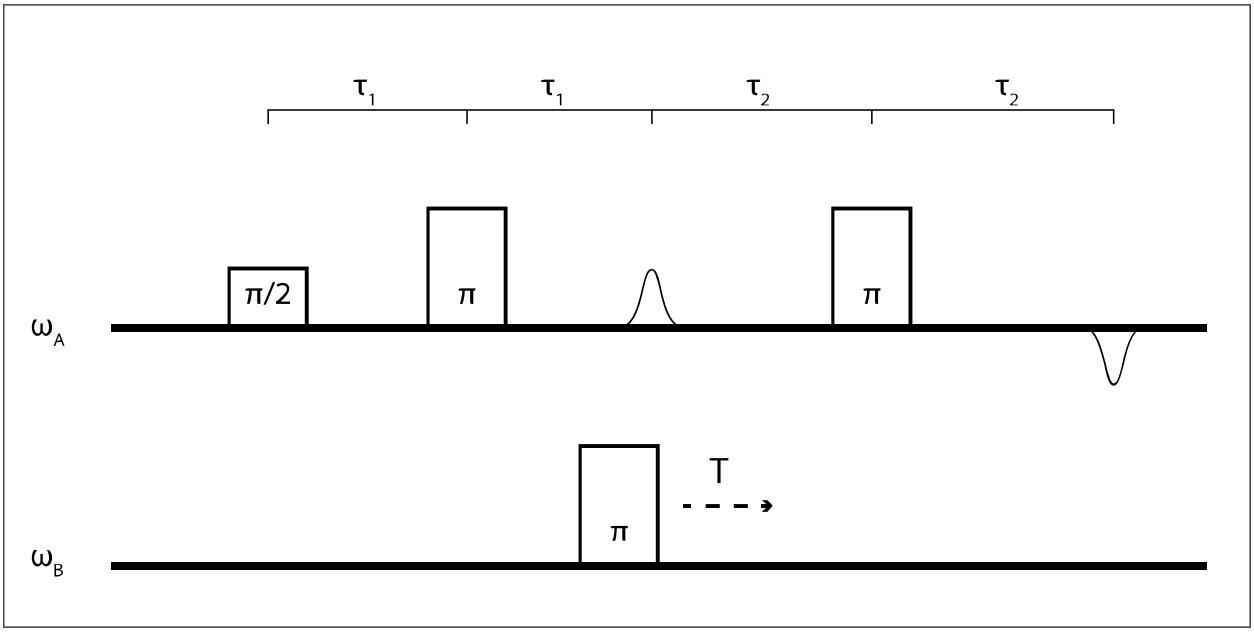

Figure 8: DEER 4-pulse sequence

unpaired electrons [40]. The range of DEER is very similar to that of the fluorescence based FRET technique which has a theoretical range of 1-10 nm [41]. The 4 pulse DEER sequence is shown in Figure 8 with a final negative echo. The experiment works best with frozen solutions (80K) because the dipolar interaction is averaged out at room temperature [42]. Another very important reason for cooling the temperature so low is that the phase memory time (T_m) of the spin label is greatly increased. The T_m is made up of several relaxation factors such as T_2 (spin-

spin relaxation), spectral, spin, and instantaneous diffusion. One way to measure the value of T_m is to create a plot of the time τ (the separation between the pulses) versus the echo amplitude and fit the curve with an exponential decay; the decay constant is the T_m value in this case. However, if the curve does not follow a monoexponential, a simpler approach is to determine the time τ it takes for the echo to reach 1/e its maximum value [33]. The longer the relaxation time, the longer the signal will take to dampen or decay.

Since DEER measures the dipolar coupling, the Hamiltonian for the interaction is the previously described but slightly modified:

$$\widehat{H}_{DC} = \frac{\hat{\mu}_A \cdot \hat{\mu}_B}{r^3} - \frac{3\langle \hat{\mu}_A \cdot \vec{r} \rangle \langle \hat{\mu}_B \cdot \vec{r} \rangle}{r^5}$$

The cross product terms in the Hamiltonian are often negligible and the reduced Hamiltonian is:

$$\widehat{H}_{DC} = \frac{g_A g_B \beta_A \beta_B}{r^3} \hat{S}_z^A \cdot \hat{S}_z^B (1 - 3\cos^2\theta)$$

In this case, the dipolar frequency can be determined by:

$$\omega_{dip} = \frac{D_{dip}}{r^3}(1 - 3\cos^2\theta)$$

where D_{dip} is the constant term calculated to equal ~2π x 52 MHz/nm^3 when g^A and g^B are equal to 2. The consequence of having the cosine term in the equation means that the values for ω_{dip} vary from $-2D_{dip} / r^3$ to $+1D_{dip} / r^3$.

There are two different pulse channels labeled ‘A’ and ‘B’ where the A channel (observer) are typically the spins with m_I of 0 and is used to monitor the dipolar coupling. The B channel

represents a second pulse channel (pump) which is in place to probe the strength of the interaction between spins 'A' and 'B'. The initial two pulses on the A channel form the previously mentioned Hahn echo.

After the echo is formed, the second pulse channel (B) becomes important. The first pulse on this channel (π) causes the 'B' spins (the spins resonant with the B channel) to flip 180° and also disrupts the precession of the 'A' spins. This pulse is stepped out (T increases) and another pulse on the A channel refocuses the initial echo. The DEER signal is a measurement of the final echo intensity which is [43]:

$$V(T) = \int P(r)dr \int_0^{\frac{\pi}{2}} \cos[(1 - 3\cos^2\theta)\omega_{AB}T] \sin\theta d\theta$$

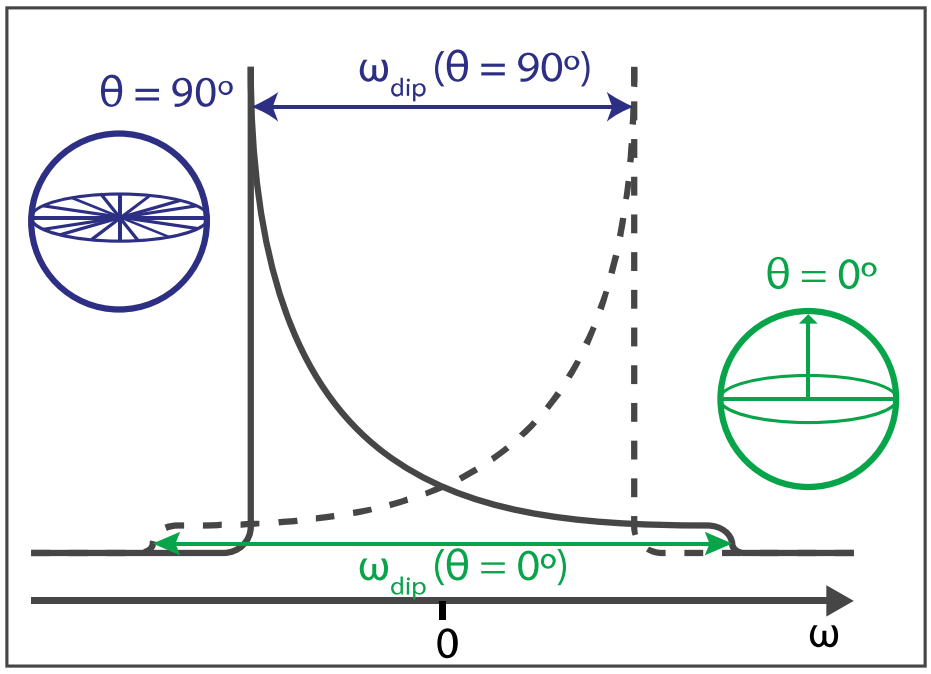

Figure 9: Pake pattern with multiple spin orientations

where V(T) is the intensity of the echo with respect to T, P(r) represents the distance distribution, and the function is integrated over all the possible orientations and distances of the spin

label (θ, r respectively). The spin label has several possible conformations that it can sample and therefore there are several possible interspin distances.

The Fourier transform of this function (from the time domain to frequency) is known as a Pake pattern (Figure 9). The data is fit using a program called DEER Analysis which can be used to generate the distance distribution P(r) from the data set [44]. Solving for P(r) is an ill-posed problem which means that small variations in the input data such as noise will have significant effects on the output data. It has been shown that one of the best processing methods is Tikhonov regularization with an added nonnegativity constraint $P(r) > 0$ [45].

The width of this distribution is directly related to the flexibility of the linker; as the flexibility of the linker increases, the width of the distribution increases. A broad distribution is not desirable because DEER measures the distances between two paramagnetic centers, such as two nitroxide radicals, and not the distance between the Cα's of the R1 groups. This distinction is important because the distance between the alpha carbons is more biologically relevant than the nitroxide, which are several bonds away from the backbone.

As more sites within the biological system are spin labeled, distance measurements between sites can be made after taking DEER measurements. These constraints can be utilized along with molecular modeling to generate and refine the structure of the system as a whole. One of the most powerful applications of DEER is for systems where other structural techniques are not possible. For example DEER has been used to determine the structure of many proteins that are hard to crystallize such as membrane proteins [46]. It has also been used to examine the open and closed states of restriction endonucleases when bound to various sequences of

DNA [47]. There are literally hundreds of examples of the utility of DEER spectroscopy in biological systems and the references here are just a small sample of the variety [45, 48-50].

The end goal for protein research using ESR is direct access to the protein backbone for dynamics studies as well as distance information. With this in mind, a shorter and more rigid linker molecule is highly desirable.

2.4. MODEL PROTEIN SYSTEM – GB1

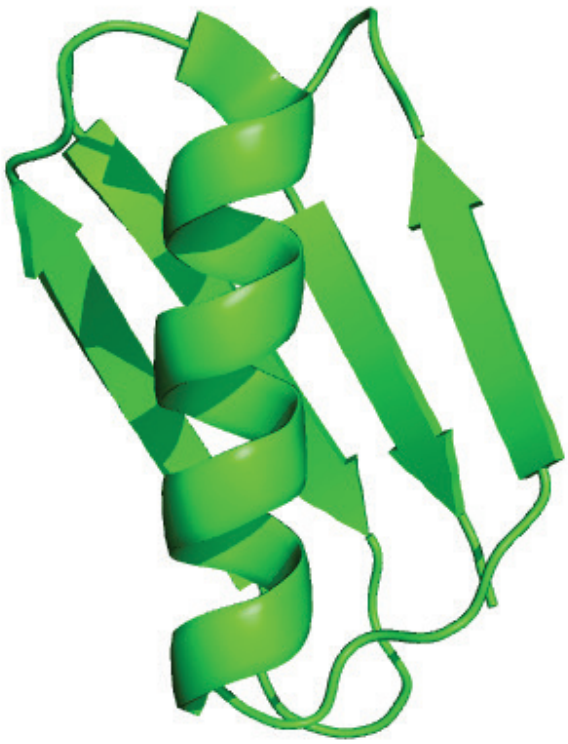

Figure 10: GB1 - PDB: 2QMT

This work will utilize the 56 amino acid residue B1 immunoglobulin-binding domain of protein G (GB1), which has been studied extensively through crystal structures, NMR structures, and various computational modeling [18, 51-56]. GB1 is used as a model system for protein folding by many groups due to its high stability [57].

A high quality crystal structure is shown in Figure 10 and shown in Figure 11 is the secondary structure diagram for wild type

GB1 [52]. One of the additional advantages to using GB1 is that it contains alpha helices, beta sheets, and loop regions making it even more ideal for multiple secondary structure analysis.

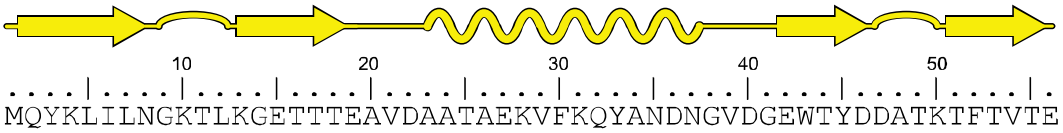

Figure 11: Secondary Structure Figure for GB1

The purification process is relatively easy and high yielding; production of the protein is not generally a limiting factor.

3.0. PRELIMINARY RESULTS

I describe herein the production, purification, and identification of several GB1 mutations as well as the modification of one of these mutations with MSH to form the desired intermediate containing dehydroalanine. Also this work will show that the subsequent reaction of dehydroalanine containing protein with a small thiol is successful proving that the protein system will be an ideal candidate for the goals described previously. Partial synthesis of a thiol containing spin label is included as well.

3.1. SITE DIRECTED MUTAGENESIS

Site directed mutagenesis involves selectively changing a residue on a protein to another residue of choice. To change a residue, the DNA sequence used by the host cell (in most cases bacteria or yeast) to produce the protein has to be modified. Changing the DNA requires a

primer, a strand of nucleic acids that is used to synthesize DNA within a biological system, the DNA itself, and deoxyribonucleotide triphosphates (dNTPs).

The DNA, primers (sense and antisense), polymerase, and dNTPs are combined into a polymerase chain reaction (PCR) tube. The system is heated to 90°C for 5 minutes to unwind the DNA into single strands. The temperature is lowered to ~60°C, depending on the primer, to allow the primer to anneal to the DNA; the mixture being called the DNA template. The temperature is raised to 72°C (depending on the polymerase used) and the polymerase binds to the newly formed DNA template. The polymerase will start synthesizing a new complementary DNA strand using the dNTPs in the 5' to 3' direction. This process is repeated for several cycles, often between 25 and 30, with each step theoretically doubling the target DNA. The PCR system finishes the process with an elongation step which will ensure that all of the single stranded DNA will be fully synthesized. The system cools to 4°C and the DNA mix can be stored indefinitely.

3.2. CELL TRANSFORMATION

A tube containing the BL21(DE3) competent *E. coli* cells is thawed on ice for 10 min. During this time, culture tubes are also chilled on ice. DNA (2 uL; 100 ng total) is added to the cell mixture. The tubes are carefully flicked 4-5 times to mix the cells and DNA. Care must be taken to not vortex the mixture as it will damage the DNA. The mixture is placed on ice for 30 minutes. The

tube is placed in a water bath at 42°C for exactly 45 seconds and then put back on ice for 5 minutes. Room temperature SOC media (900 uL) is added to the mixture and incubated with shaking (250 rpm) at 37°C for 60 minutes. During this time agar plates containing ampicillin are warmed to 37°C in an incubator. The cells are then mixed by inverting the tube and an aliquot (100 uL) is diluted 10 fold with SOC. Diluted and concentrated cells (100 uL each) are spread onto plates and left to grow overnight at 37°C. The cells will only grow if they have taken up DNA as the plasmid contains a gene that codes for ampicillin resistance.

3.3 RESTRICTION ENZYMES AND GELS

In order to confirm that the overnight cultures have produced the desired mutation, they are selected with a sterile toothpick and added to a culture tube with SOC media (5 mL). The tubes are incubated overnight at 37°C with shaking (250 rpm) and the DNA extracted the following day with a Qiagen miniprep kit. The DNA is eluted in sterile distilled water (50 uL) in the final step. The extracted DNA is combined with the appropriate restriction enzyme that corresponds to the silent mutation utilized in that mutant and heated to 37°C in the PCR for 2 hours. After the digest, DNA (5 uL) is combined with loading buffer (5 uL) containing colored dyes to monitor the running progress of the gel and water (5 uL). The agarose gel contains ethidium bromide which will glow under UV light when bound to DNA. Most commonly the gel is comprised of ~1% agarose in water; a higher percentage agarose leads to longer gel running times and better

resolution in the lower weight range. The gels are analyzed and compared with wildtype (WT) DNA which has been digested concurrently.

The following gels (Figure 12**,** Figure 13) are shown with their respective band sizes from the mutations that have been successful thus far by this author.

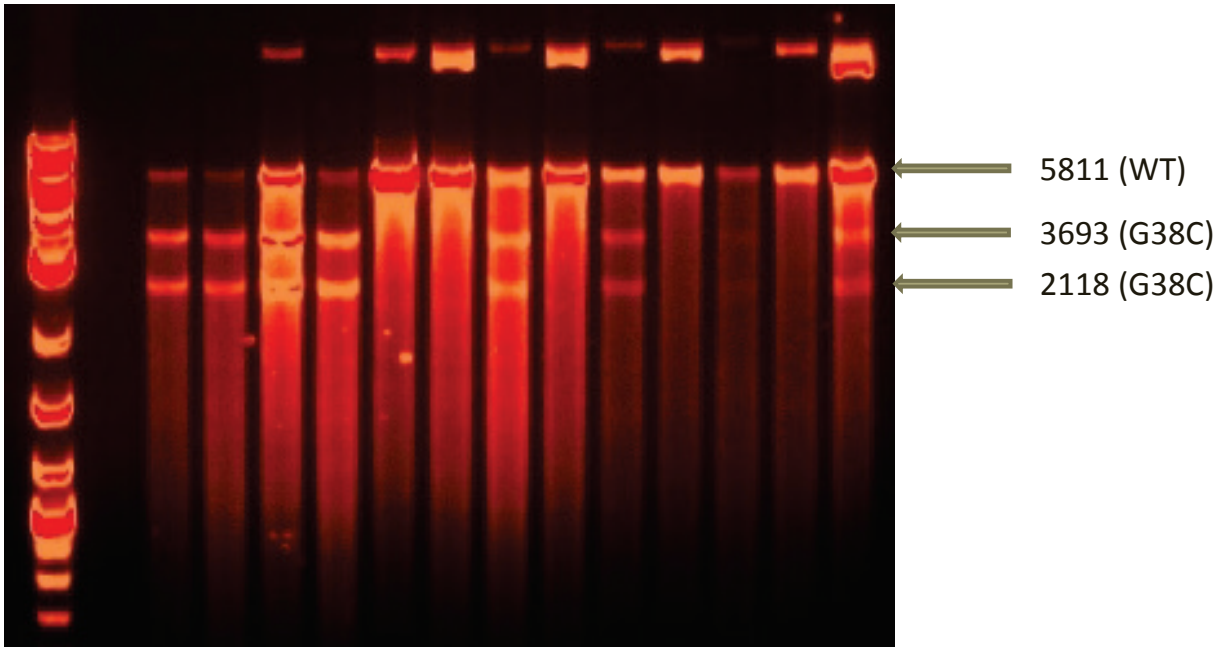

Figure 12: Gel with G38C mutation

3.4. PROTEIN PRODUCTION AND PURIFICATION

Protein production is described in detail in a recently published work by the Saxena group including this author [18]. The plasmid containing the mutated DNA was transformed into BL21(DE3) *E. coli* cells as previously described and then grown in LB media (1 L) with ampicillin (100 ug/mL). The mixture was shaken at 37°C until the OD_{600} was between 0.6 and 0.8. At this

point IPTG was added to a final concentration of 500 uM to induce protein production. After 4 hours of growth, the cells were harvested with centrifugation. The pellet was resuspended in 20 mM Tris-HCl (pH 8.5), 5 mM NaCl, 5 mM $MgCl_2$ 1 mM $CaCl_2$, 1 mg/mL lysozyme, 11 units/mL DNase I, 1.3 units/mL RNase A, and 0.1% w/v Triton X-100. The cells were shaken on ice for 60 minutes and then sonicated 3 x 30s to lyse the cells. The cells were then centrifuged again at

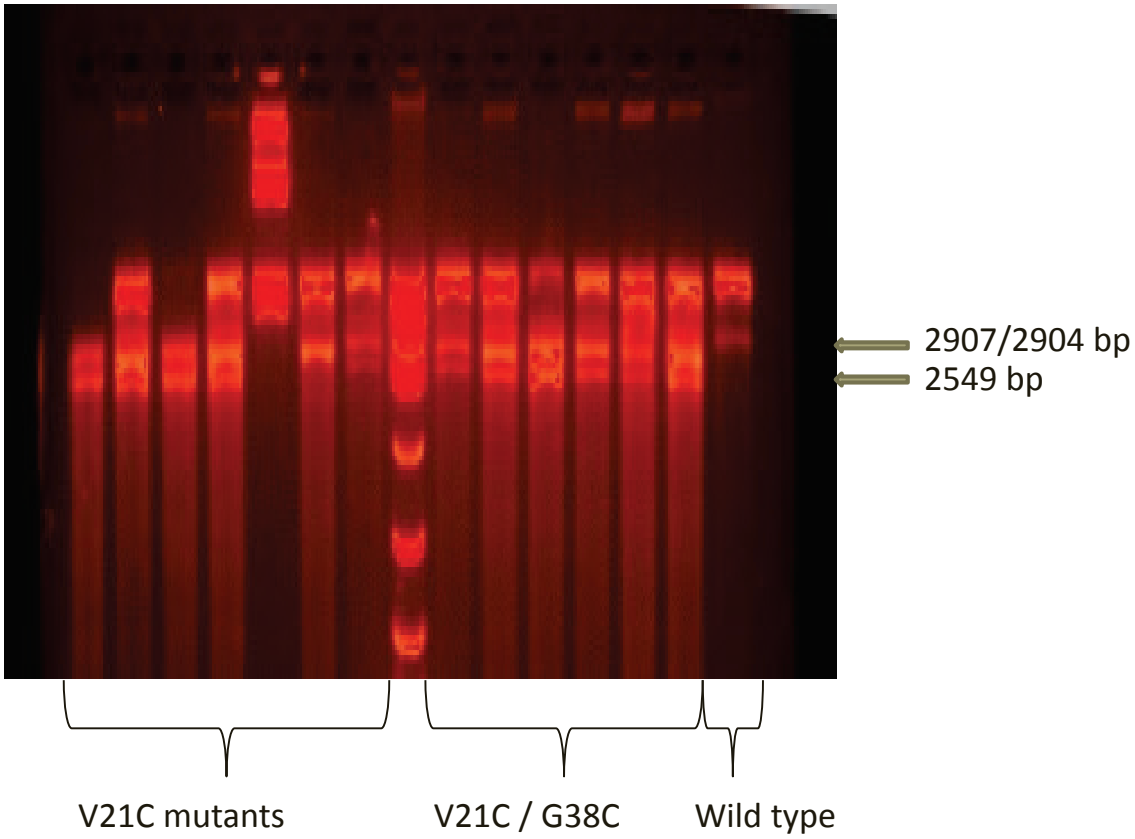

Figure 13: Gel with V21C and V21C/G38C mutations

20,000 rpm and the supernatant was collected and placed into a water bath at 80°C for 10 minutes. After that, the mixture was centrifuged again at 20,000 rpm and the supernatant was sterile filtered with a 0.22 um filter.

The supernatant was loaded onto a GE-Healthcare HiTrap Q HP column that had been equilibrated in 20 mM Tris-HCl (pH 8.5) with 5 mM NaCl. The concentration of NaCl was increased over 40mL to 500 mM and individual peaks were collected to be analyzed using SDS-PAGE gels. The fractions that contain GB1 were combined and concentrated using an Amicon 3000 MWCO centrifuge filter. Then TCEP was added to a final concentration of 10 mM and loaded onto a size exclusion column (GE Healthcare Sephacryl S-100 26/60) that had been equilibrated in 50 mM sodium phosphate (pH 6.5) with 150 mM NaCl. Fractions were again checked with SDS-PAGE gels and the GB1 containing fractions were combined, concentrated to 1 mg/mL with 10 mM TCEP and 20% glycerol, and flash frozen in liquid nitrogen for long term storage at -80°C.

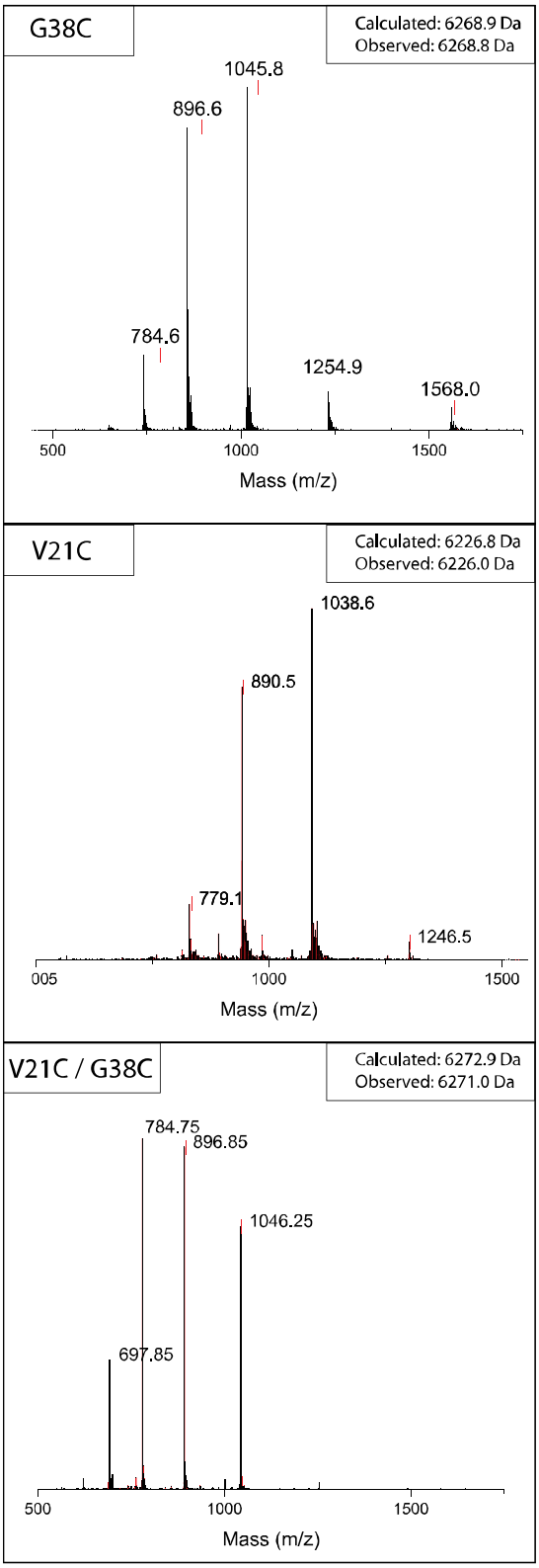

Figure 14: HPLC-MS spectra for each of the successful mutations

3.5. CONFIRMING PROTEIN IDENTITY

Protein identity was confirmed using mass spectrometry using high pressure liquid chromatography mass spectrometry (HPLC-MS). A small amount of purified protein (5 uL) was injected onto an LCM-2020 (Shimadzu) equipped with Electrospray ionization (ESI). Protein was assigned based on 4 different multiply charged peaks using ESIprot [58]. Figure 14 contains the HPLC-MS spectra for each of the mutations successfully purified.

3.6. MSH REACTION

Synthesis of O-mesitylenesulfonylhydroxylamine (MSH) is described in previous work by the Davis group [25]. Proton and carbon nuclear magnetic resonance (δ) was recorded on a Bruker Avance III

(400 MHz, 100 MHz for proton and carbon respectively) spectrometer or a Bruker DRX (300 MHz, 75 MHz) spectrometer as noted.

3.6.1. Synthesis of MSH-precursor

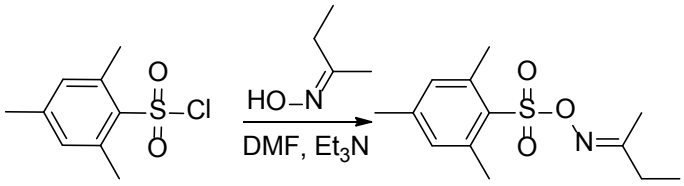

Ethyl N-hydroxyacetimidate (2.32g, 22.5 mmol) was dissolved in DMF (5.9 mL, 3.8M). Triethylamine (3.1 mL, 22.5 mmol) was added and the solution was cooled to 0°C. Then 2-mesitylenesulfonyl chloride (4.92g, 22.5 mmol) was added and the mixture stirred vigorously for 15 min. The mixture was then diluted with dichloromethane (100 mL) and washed with water (100 mL x10). The organic layer was dried with $MgSO_4$, filtered, and the solvent removed with reduced pressure. Spectroscopic data similar to literature values: ^{1}HNMR (400 MHz, $CDCl_3$), δ 6.97 (s, 2H), 3.91 (q, J = 7 Hz, 2H), 2.65 (s, 6H), 2.31 (s, 3H), 2.04 (s, 3H), 1.19 (t, J = 7 Hz). Yield = 3.52g (55%). The material was carried through without further purification.

3.6.2. Synthesis of MSH

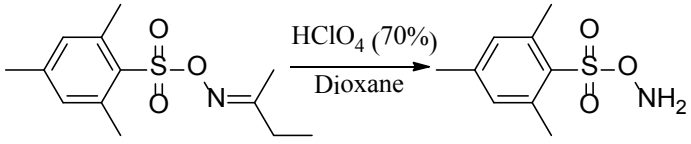

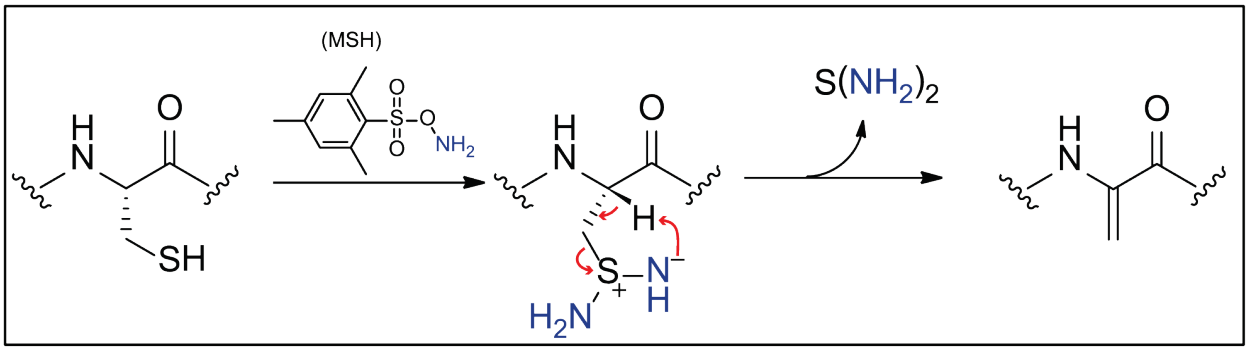

Figure 15: Conversion of cysteine (left) using MSH (middle) to dehydroalanine (right)

MSH precursor (3.5159g, 12.3 mmol) was dissolved in dioxanes (3.17 mL, 3.8M) and cooled to 0°C, Then $HClO_4$ (70%, 1.43 mL) was added dropwise while stirring. After 2 minutes of stirring the mixture solidified. The mixture was added to ice water (100 mL) and the flask rinsed with water (50 mL), ether (50 mL), and extracted with ether (50 mL). The organic layer was partially neutralized and dried with potassium carbonate (AH) and filtered. The filtrate was concentrated to less than 100 mL and then added to 150 mL of ice cold hexanes and allowed to crystallize. The product was a whitish solid that was dried under reduced pressure and stored at -20°C. The NMR was consistent with literature: ^{1}HNMR (400 MHz, $CDCl_3$), δ 6.82 (s, 2H), 4.38 (br s, 4H), 2.50 (s, 6H), 2.25 (s, 3H). Yield = 2.20g (83%).

3.6.3. Reaction with MSH

For the conversion of cysteine to dehydroalanine using MSH (mechanism in Figure 15), the following procedure was used. A 1 mg/mL aliquot of mutant GB1 (160 uM) that had been previously stored in 50 mM sodium phosphate (pH 6.5) with 20% glycerol and 10 mM TCEP was buffer exchanged using 5 x 5 mL GE Healthcare HiTrap Desalting columns previously equilibrated with 50 mM sodium phosphate (pH 8.0). The protein was eluted over 4mL and was not concentrated further. MSH (100X protein concentration, 3.5mg, 16.1 umole) was dissolved in DMF (100 uL) and added to the eluted protein and vortexed for a minute. Then the protein was shaken in a fridge for 2 hours and then syringe filtered (0.22 um). The filtrate was then

concentrated using an Amicon 3,000 MWCO centrifuge filter and desalted using the same column as previous. The protein was analyzed using HPLC-MS to confirm the modification was successful (Figure 16).

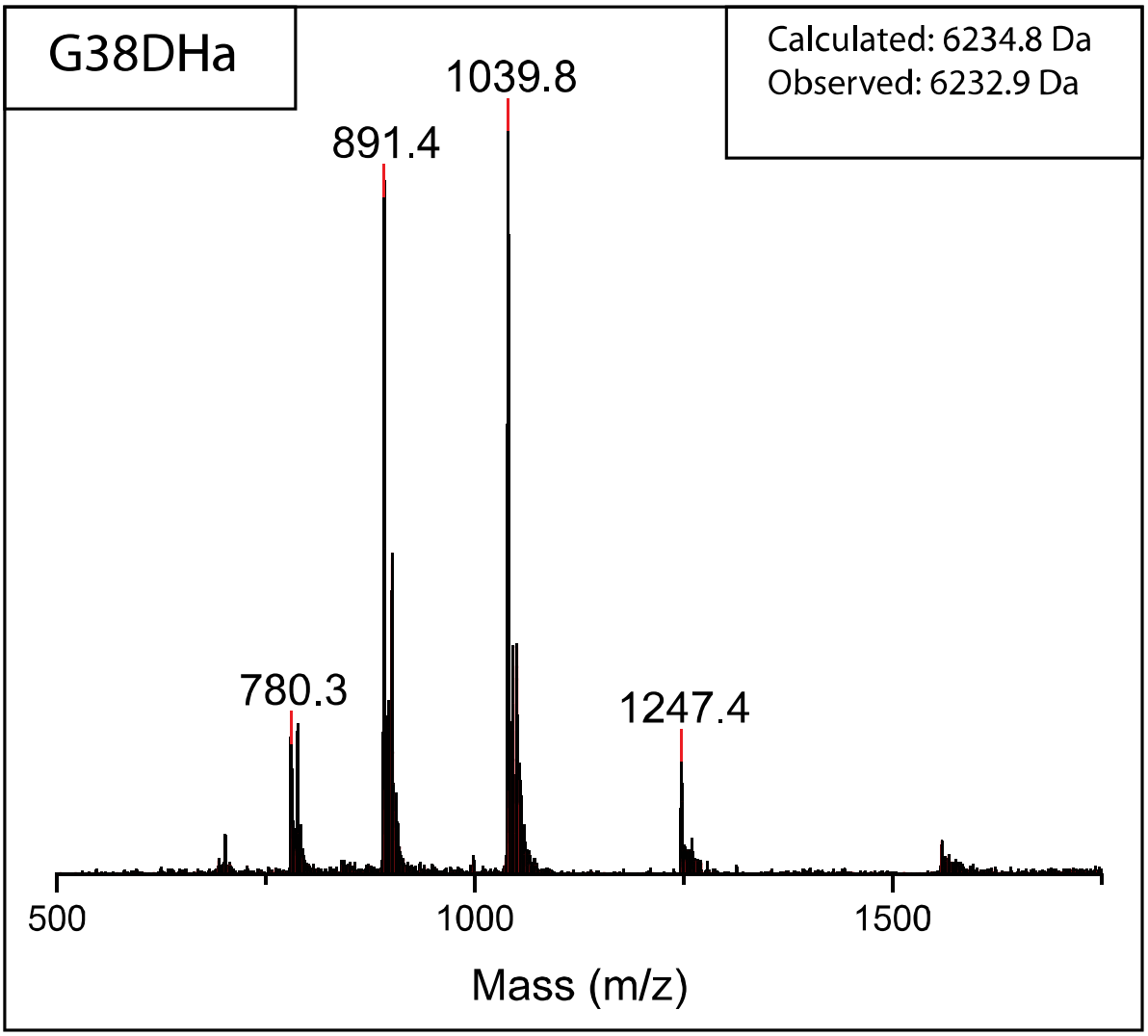

Figure 16: HPLC-MS spectrum for successful conversion of cysteine to dehydroalanine

3.6.4. Ethanethiol experiment

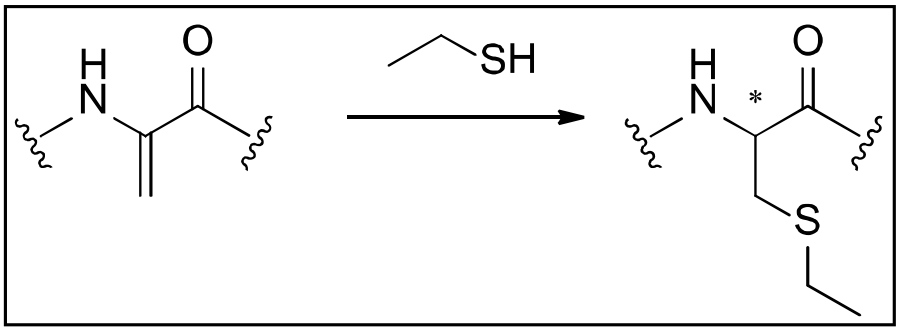

Figure 17: Michael addition of ethanethiol to dehydroalanine

The Michael addition of a thiol to dehydroalanine was tested using ethanethiol (Figure 17). A small aliquot (10 uL) of ethanethiol was added to an aliquot of G38DHa (100 uL) and vortexed for a minute. Then then mixture was analyzed using HPLC-MS to confirm the addition of

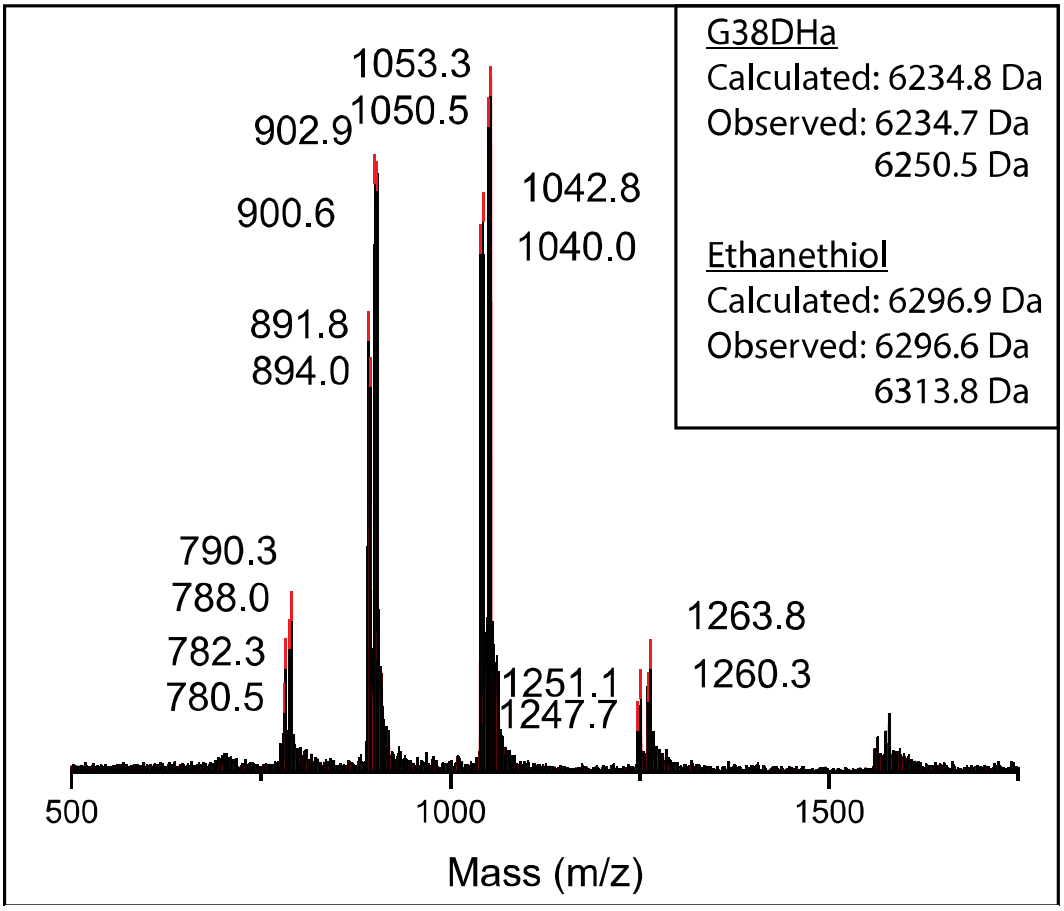

Figure 18: HPLC-MS spectrum for the Michael addition of ethanethiol to dehydroalanine

ethanethiol to the protein (Figure 18). Unfortunately the protein had been left to react with MSH overnight and contained an impurity that was 16 Da higher mass than dehydroalanine. Despite the impurity, the addition of ethanethiol was successful indicating that the increase in mass was not due to hydration of the dehydroalanine to serine. The impurity is likely either amination of the methionine residue since MSH is an aminating reagent. This hypothesis is supported by the literature and can be removed using TCEP or DTT [26].

3.7. DMDO EXPERIMENT

One of the hurdles to overcome in the synthesis of new spin labels is that the radical in the nitroxide is very reactive and will oxidize free thiols [59]. Since the mode of attachment using dehydroalanine is a free thiol, a new approach was needed. One way to solve this issue is synthesizing a spin label precursor that needed to be oxidized in order to be activated. One such oxidant is dimethyldioxirane (DMDO) and has been shown to oxidize piperidine spin label precursors to nitroxide radicals [60]. DMDO was utilized with several functional groups often found in protein systems (carboxylic acids, amines, alcohols, and

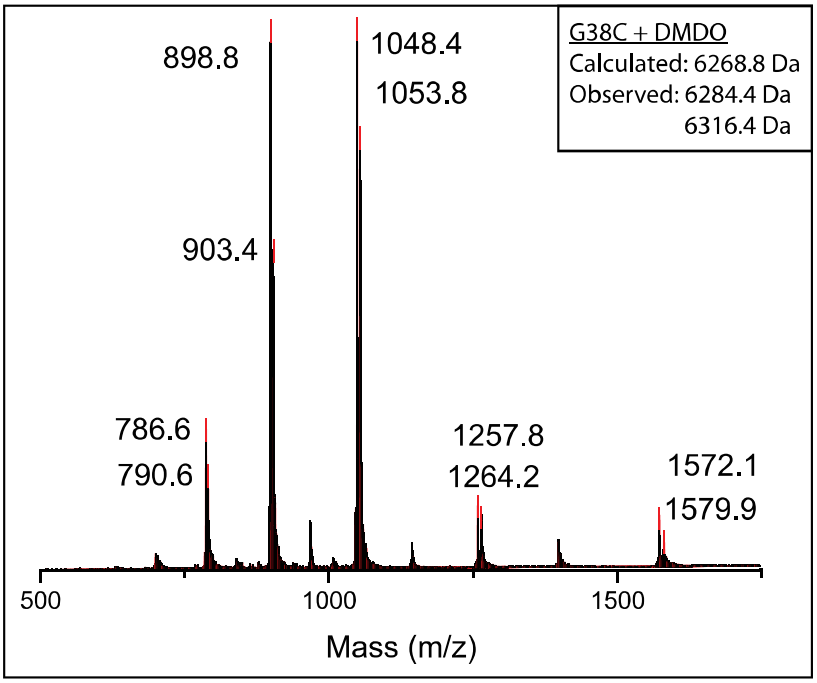

Figure 19: HPLC-MS spectrum for the addition of DMDO to G38C

esters) with only oxidation of the nitrogen to a hydroxylamine and then to a nitroxide radical. With this in mind, the applicability of DMDO as a possible oxidant needed to be tested to ensure that the protein itself would not be over oxidized or damaged. The procedure developed is to use two equivalents of DMDO per equivalent of starting material [61]. Therefore despite changing the system, the same equivalents of DMDO will be utilized here.

DMDO is unstable; the reaction to generate it is very low yielding and is only obtained as a solution in acetone (~0.1M). However, DMDO can be generated in situ by adding acetone to an aqueous solution with oxone and sodium bicarbonate [62]. An aliquot of G38C (1 mg/mL) was desalted into 50 mM sodium phosphate (pH 8.0) as described previously. A small amount of DMDO (0.2 uL) was added to an aliquot of the purified protein (300 uL) and shaken for an hour. The mixture was analyzed by HPLC-MS and two oxidation products were seen (+16 and +48 Da from G38C, Figure 19) related to the likely oxidation of cysteine to sulfenic acid and sulfonic acid respectively.

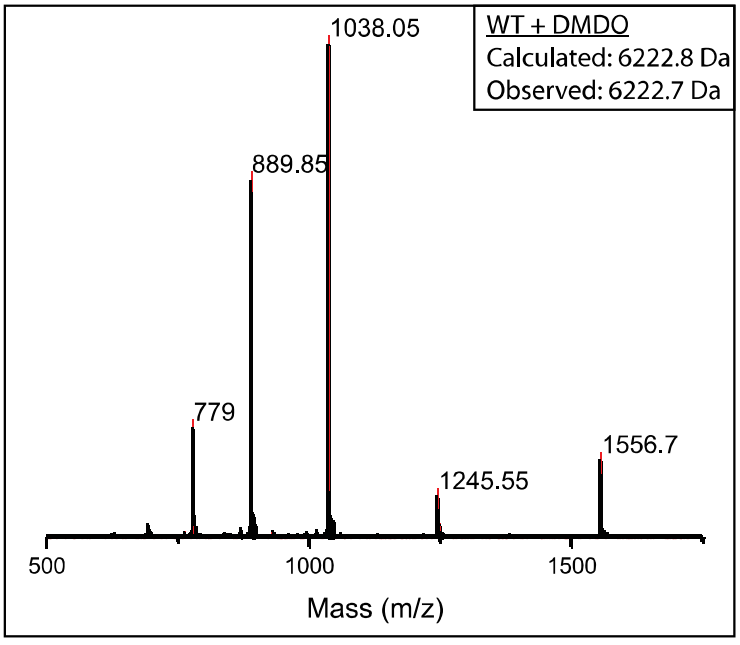

Figure 20: HPLC-MS spectrum for the addition of DMDO to WT GB1

The next step was to test WT to ensure that the cysteine was the oxidized species and there was no oxidation of the methionine. As previous, an aliquot of the protein was desalted and reacted with DMDO for an hour. The mixture was again analyzed using HPLC-MS and

fortunately no oxidation was observed (Figure 20). The experiment proves that DMDO is suitable in a protein environment and will not damage the protein under the conditions tested.

3.8. SYNTHESIS OF SPIN LABELS

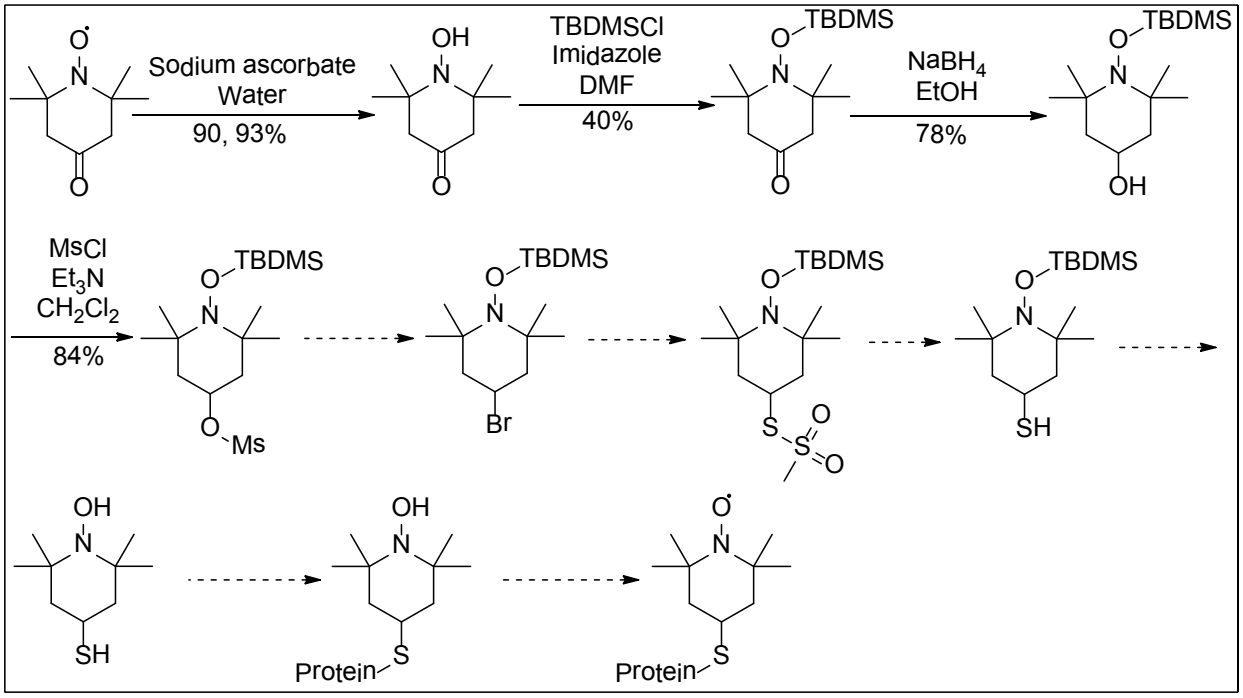

Figure 21: Reaction scheme for this work

The synthetic goals of this work are shown in Figure 21 where the solid arrows indicate the reaction conditions and yield and the dashed arrows indicate proposed pathways. Once the thiol is synthesized, it can be attached to a protein with either traditional labeling to form a disulfide bond or attached to dehydroalanine.

3.8.1. 1-Hydroxy-2,2,6,6-tetramethylpiperidin-4-one (**1**)

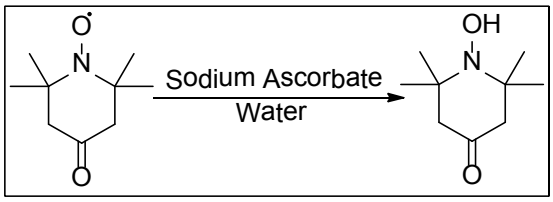

Figure 22: Reduction of radical

Sodium ascorbate (1.97g, 9.95 mmol) was dissolved in water (17 mL, 0.35M). While stirring, 1-oxyl-2,2,6,6-tetramethylpiperidin-4-one (1.03g, 6.03 mmol) was added. After 10 min of stirring, 2 mL of NaOH (10%) was added. Initially the starting material was suspended in solution but became homogeneous and yellow after 10 min of stirring. Upon addition of NaOH, the solution became a deep red. The mixture was extracted with 100 mL of ethyl acetate and washed with brine (50 mL x2). The organic layer was dried with $MgSO_4$, filtered, and the solvent was removed under reduced pressure. Yield = 0.96g (93%). Spectroscopic data was identical to previously reported [63]. ^{1}HNMR (400 MHz, $CDCl_3$) δ 4.43 (s, 1 H), 2.41 (s, 4 H), 1.22 (s, 12 H). ^{13}CNMR (100MHz, $CDCl_3$) δ 207.9, 61.9, 53.4, 26.5. HRMS *m/z* calculated for [$C_9H_{18}NO_2$] 172.1338; found 172.1305.

3.8.2. 1-((Tert-butyldimethylsilyl)oxy)-2,2,6,6-tetramethylpiperidin-4-one (**2**)

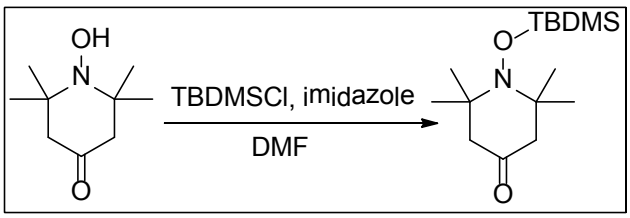

Figure 23: Protection of hydroxylamine

1-Hydroxy-2,2,6,6-tetramethylpiperidin-4-one (0.96g, 5.61 mmol), imidazole (1.22g, 17.95 mmol), and TBDMSCl (1.35g, 8.98 mmol) were added and while stirring under N_2 DMF (4.08 mL, 1.38M) was added. The reaction was stirred for 2 days and diluted with 30 mL hexanes and washed with water (50 mL x3). The organic layer was dried with $MgSO_4$, filtered, and the solvent was removed under reduced pressure. The crude material was purified using flash chromatography with gradient elution from 1-5% ether/hexanes. Yield = 0.63g (40%). Spectroscopic data was consistent with literature [64]: ^{1}HNMR (400 MHz, $CDCl_3$), δ 2.70-2.10 (m, 4 H), 1.19 (s, 12 H), 0.98 (s, 9 H), 0.21 (s, 6 H). ^{13}CNMR (100 MHz, $CDCl_3$), δ 208.3, 63.2, 53.7, 26.8, 19.3, -1.9. HRMS *m/z* calculated for [$C_{15}H_{32}NO_2Si$] 286.2202; found 286.2205.

3.8.3. 1-((Tert-butyldimethylsilyl)oxy)-2,2,6,6-tetramethylpiperidin-4-ol (**3**)

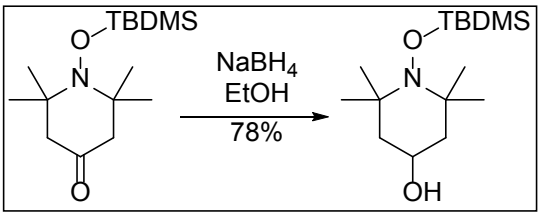

Figure 24: Reduction of ketone

Procedure adapted from literature [65]: 1-((tert-butyldimethylsilyl)oxy)-2,2,6,6-tetramethylpiperidin-4-one (0.51g, 1.7 mmol) was stirred on ice in ethanol (17 mL, 0.1M). $NaBH_4$ (0.02g, 0.44 mmol) was added and stirred for 1 hour. The solution was diluted with brine (50 mL) and extracted with ethyl acetate (50 mL). The organic layer was dried with $MgSO_4$, filtered, and the solvent was removed under reduced pressure. Yield = 0.40g (78%). ^{1}HNMR (400 MHz, $CDCl_3$), δ 3.96 (m, 1 H), 1.83 (dd, J = 3.26, 11.92 Hz, 2 H), 1.45 (t, J = 11.80 Hz, 2 H),

1.15 (s, 6H), 1.12 (s, 6H), 0.96 (s, 9 H), 0.16 (s, 6 H). ^{13}CNMR (100 MHz, $CDCl_3$), δ 63.2, 60.3, 48.7, 34.5, 26.9, 19.4, -2.0. HRMS *m/z* calculated for [$C_{15}H_{34}NO_2Si$] 288.2359; found 288.2353.

3.8.4. 1-((Tert-butyldimethylsilyl)oxy)-2,2,6,6-tetramethylpiperidin-4-yl methanesulfonate (**4**)

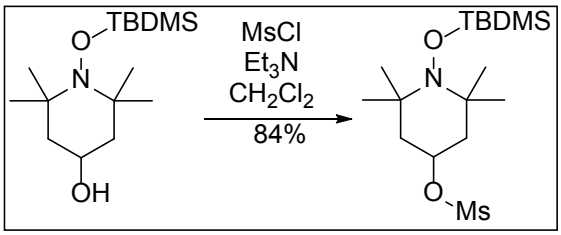

Figure 25: Mesylation of alcohol

Procedure adapted from literature [66]: 1-((tert-butyldimethylsilyl)oxy)-2,2,6,6-tetramethylpiperidin-4-ol (0.20g, 0.7 mmol) was dissolved in dichloromethane (4.7 mL, 0.15M). While stirring under N_2, triethylamine (0.11 mL, 0.77 mmol) and MsCl (0.06 mL, 0.8 mmol) were added at 0°C. The mixture was stirred for 2 hours at room temperature. The reaction was diluted with water (20 mL) and extracted. The organic layer was dried with $MgSO_4$, filtered, and the solvent removed under reduced pressure. Yield = 0.21g (84%). ^{1}HNMR (400 MHz, $CDCl_3$), δ 4.91 (m, 1 H), 3.00 (s, 3 H), 2.01 (d, J = 11.7 Hz, 2 H), 1.75 (t, J = 11.9 Hz, 2 H), 1.19 (s, 6H), 1.15 (s, 6H), 0.96 (s, 9H), 0.16 (s, 6H). ^{13}CNMR (100 MHz, $CDCl_3$), δ 75.1, 60.4, 45.4, 38.9, 34.4, 26.9, 19.4, -2.0. HRMS *m/z* calculated for [$C_{15}H_{34}NO_2Si$] 288.2359; found 288.2353.

3.9. ESR RESULTS

All ESR experiments were performed on a Bruker Elexsys 580 spectrometer with a Bruker ER4118X-MD5 resonator. The temperature for all experiments was controlled with an Oxford ITC503 temperature controller and an Oxford ER 4118CF gas flow cryostat.

3.9.1. MTSSL labeling

An aliquot of G38C was desalted using the methods described earlier in 50 mM sodium phosphate (pH 6.5) and 150 mM NaCl. The protein was reacted with MTSSL at a ratio of 1:10 (protein:MTSSL) and left to shake overnight at 4°C. The protein was concentrated to less than 1 mL with an Amicon 3,000 MWCO centrifuge filter and desalted again to remove the excess spin label. The protein was concentrated to 0.25 mM and diluted with glycerol to a final glycerol concentration of 20% (v/v).

3.9.2. CW-ESR

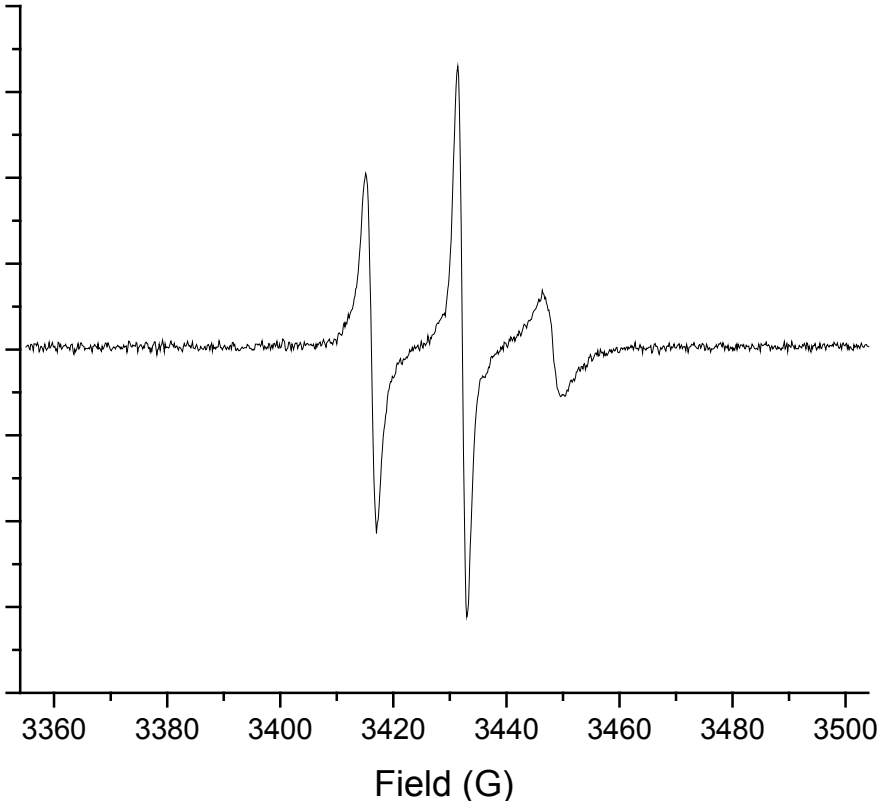

Figure 26: Room temperature CW-ESR spectrum for G38R1

Approximately 10 uL of the concentrated protein was drawn into a quartz capillary tube (1.0 o.d. x 0.8 i.d.) for room temperature CW measurements. Spectra were collected at an incident microwave power of 0.1995 mW. The modulation frequency was set to 100 kHz and the amplitude to 1 G. The room temperature spectrum is shown in Figure 26. This spectrum was taken to be used as a comparison with other labeling methods once they have been developed.

3.9.3. Double electron electron resonance (DEER)

An aliquot of V21C/G38C was desalted using the methods described earlier in 50 mM sodium phosphate (pH 6.5) and 150 mM NaCl. The protein was reacted with MTSSL at a ratio of 1:10 (protein:MTSSL) and left to shake overnight at 4°C. The protein was concentrated to less than 1 mL with an Amicon 3,000 MWCO centrifuge filter and desalted again to remove the excess spin label. The protein was concentrated to 0.25 mM and diluted with glycerol to a final glycerol concentration of 20% (v/v). The sample was transferred to a quartz MD5 EPR tube and flash frozen in liquid nitrogen.

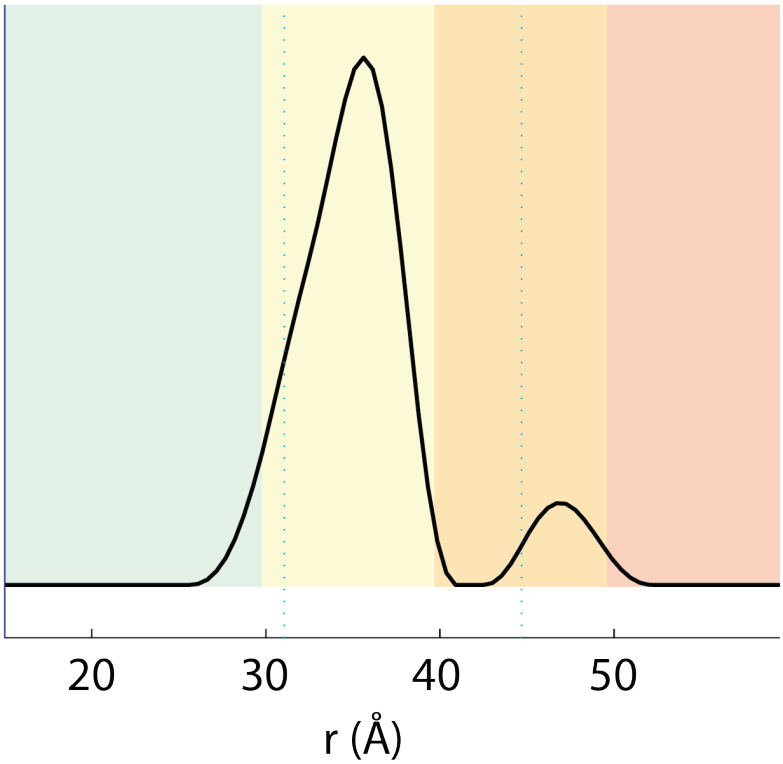

Figure 27: DEER distribution for V21C/G38C

The pulse sequence for this experiment was $\left(\frac{\pi}{2}\right)\nu_1 - \tau_1 - (\pi)\nu_1 - T - (\pi)\nu_2 - \tau_2 - (\pi)\nu_1 - \tau_2 - echo$ as was used previously and described earlier in this work [18]. The pump frequency (ν_2) was placed at the maximum of the nitroxide spectrum, and the observer frequency (ν_1) was offset 67 MHz (the maximum for the low magnetic field component). The length of the $(\pi/2)\nu_1$ and $(\pi)\nu_1$ pulses were set to 16 and 32 ns respectively and the $(\pi)\nu_2$ pulse was set to 20 ns. τ_1 was set to 200 ns while T was 128 with a incrementing stepsize of 8 ns for 128 points. τ_2 was adjusted such that $T + \tau_2 = 1200$ ns. The raw time domain DEER spectrum was analyzed using DEER Analysis 2011 [44]. The distance distribution generated from this analysis is shown in Figure 27. The breadth of the distribution is indicative of the rigidity of the linker and will be used as a comparison to synthesized spin labels.

4.0. FUTURE DIRECTIONS

One of the main goals of this work is to complete the synthesis of the desired spin labels. The proposed steps are in place and need to be completed in order to be applied to the protein system. Once the thiol spin label precursor (Figure 28) has been synthesized, it can be incorporated into a dehydroalanine containing protein sample. This sample could also be added to an unmodified protein as the thiol would react with the cysteine. Then, once attached, DMDO would be added to the system to generate the radical *in situ*.

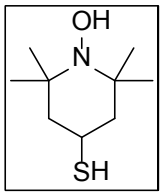

Figure 28: Thiol spin label precursor

After the proposed synthesis is completed, additional labels with bulky substituents will be synthesized in the search for the most rigid linker. The addition of a phenyl ring can add to the steric hindrance of the label and can lead to a decrease in rotational freedom. Another aspect of this work focuses on comparing ring sizes so 5 membered rings (pyrrolines) will eventually have to be synthesized as points of comparison unless they are commercially available. They will be structurally similar to the piperidines that have already been proposed so the comparison can be as direct as possible.

Another important goal is recollecting all CW-ESR data at variable temperatures and in a more viscous buffer (30% Ficoll 70), which will reduce the rotational correlation rate of the nitroxide

as described earlier in this text. By reducing the rotational correlation time and using the same mutation, the mobility of the label itself can be examined. The mobility of the site of the mutation can then be analyzed if the flexibility of the linker is known.

In addition to synthetic goals, there are still several biochemical goals left unfinished. In the subsequent paper from the Davis group [26], they describe multiple routes to dehydroalanine which could prove to be easier than using MSH. As described in this work, there are side products associated with reacting with MSH for too long. It would also be worth pursuing any other routes to artificial amino acids that could be utilized for spin labeling.

Another avenue is determining what other nucleophiles are able to react with dehydroalanine. The only nucleophiles tested in the work from the Davis group are free thiols. It is possible that free amines would work but at a much lesser reaction rate. To test this hypothesis, a dehydroalanine derivative would be used since the reaction conditions could be changed more easily than in a protein system. Additionally, the reaction products could be analyzed more absolutely since they could theoretically be crystallized to check stereochemistry.

The use of peptide synthesis could also be explored as collaborators in the Horne research group also work with GB1. Using peptide synthesis, TOAC could be engineered into the loop region (where DHA will be incorporated) as a comparison to an extremely rigid spin label. One of the disadvantages to using TOAC is that it is currently impossible to incorporate this functionality into an expressed protein. However, one possible way to engineer TOAC would be using a protein auxotroph, which would be unable to synthesize an amino acid and would only grow when given a supply of that amino acid or an analog. There are several limitations to this

approach and it would be difficult to determine if the host would actually use the artificial amino acid. It would be very interesting to incorporate TOAC into a protein that is too large to synthesize using solid phase synthetic techniques using an auxotroph.

The main direction for this work is the design and incorporation of rigid spin labels. The synthetic goals will likely evolve as more ESR data are collected. As for biochemical goals, the field is ever expanding with modifications of full length proteins become more prevalent. The conversion to dehydroalanine has been shown in GB1 in this work and various routes to this product will be explored. After the spin label has been introduced into the dehydroalanine system, and the ESR measurements have been taken, we will know the true power of this approach.

APPENDIX A. SPECTROSCOPIC DATA

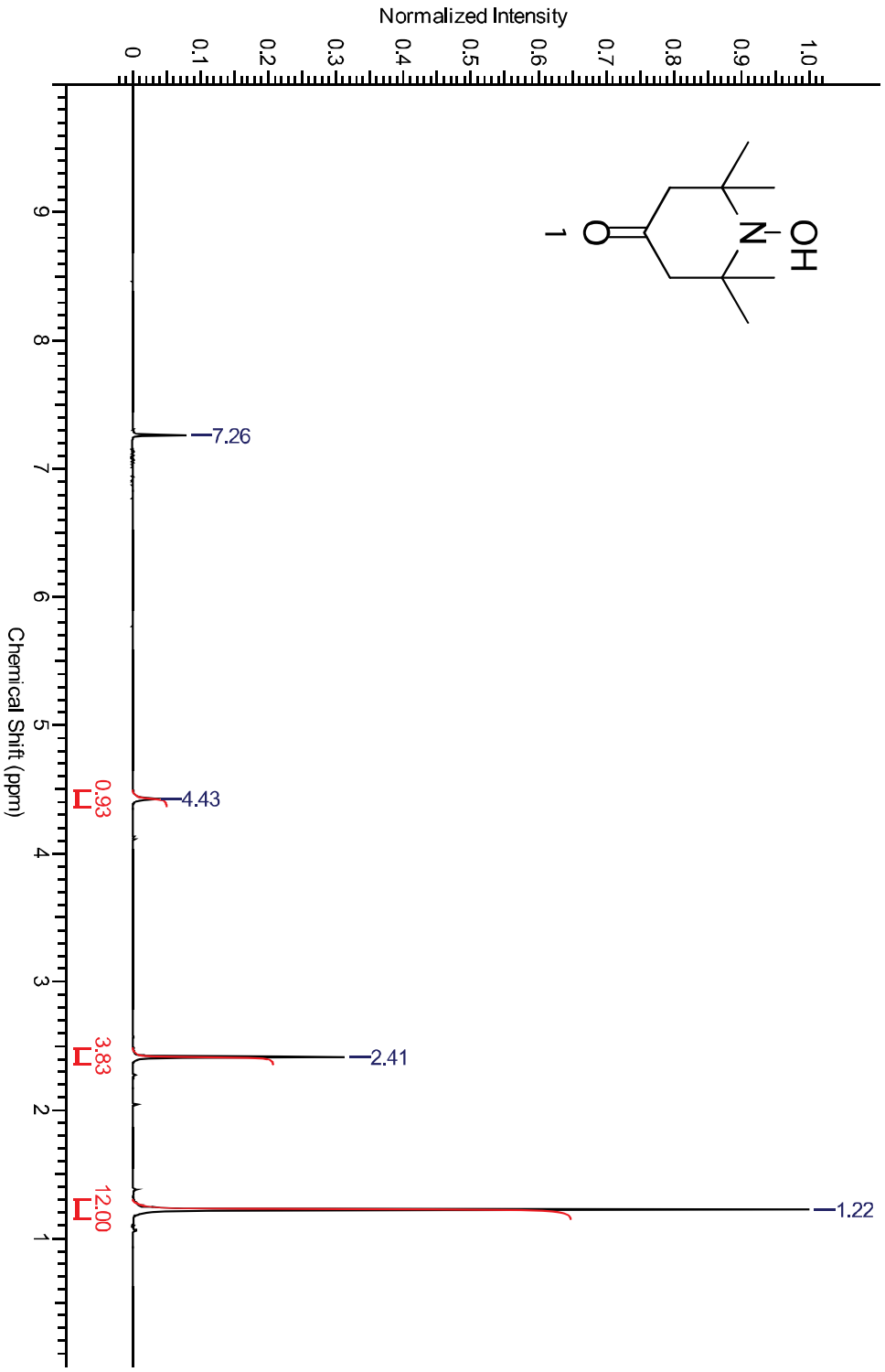

Figure 29: ^{1}HNMR of 1

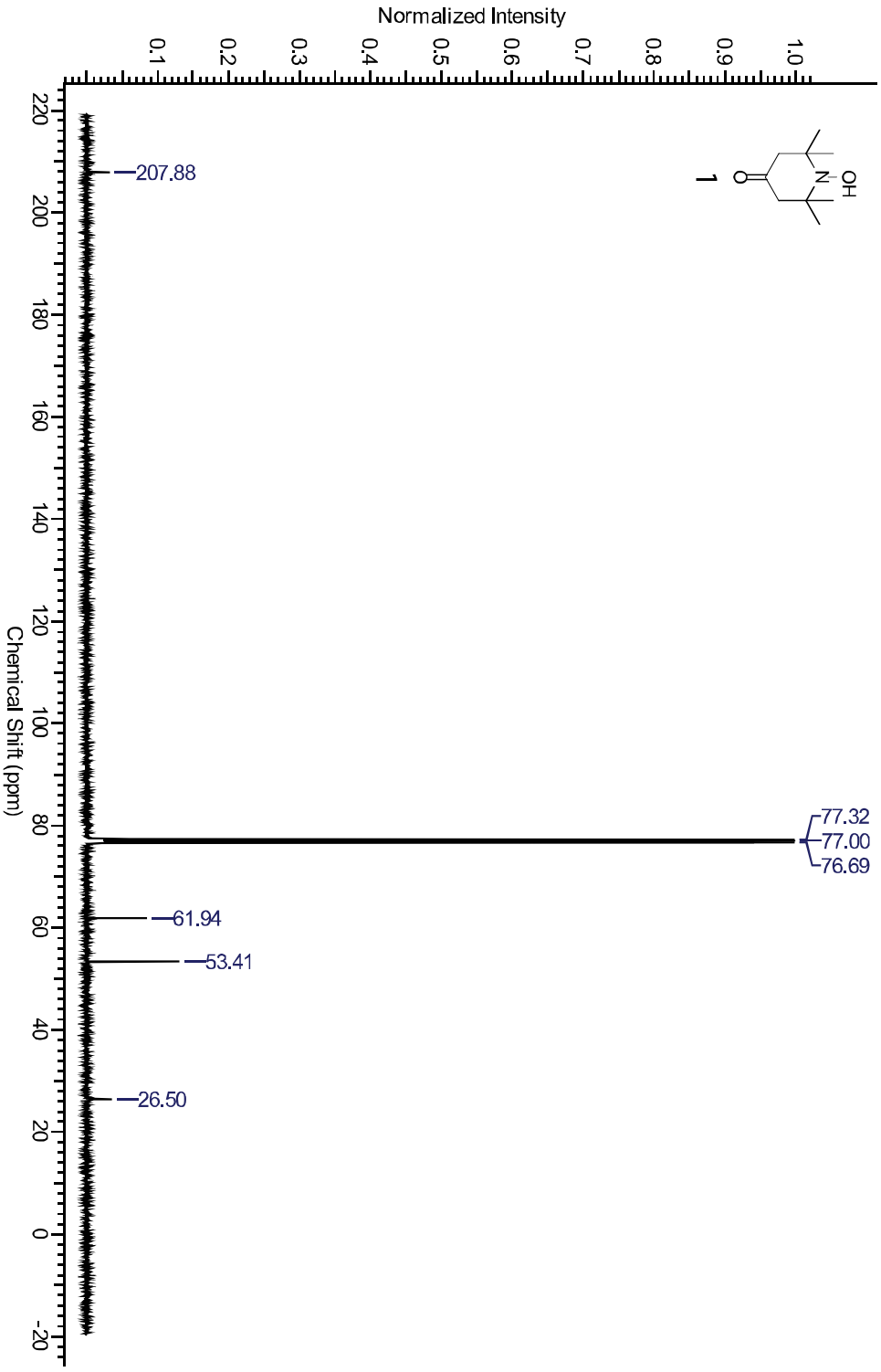

Figure 30: ^{13}CNMR of 1

Single Mass Analysis

Tolerance = 1000.0 PPM / DBE: min = -1.5, max = 100.0
Element prediction: Off
Number of isotope peaks used for i-FIT = 4

Monoisotopic Mass, Even Electron Ions
6 formula(e) evaluated with 1 results within limits (all results (up to 1000) for each mass)
Elements Used:
C: 0-9 H: 0-18 N: 0-1 O: 0-2

MSM-093
69641ASAP 310 (5.832) AM (Cen,3, 80.00, Ar,8000.0,311.08,0.00); Sm (SG, 5x3.00); Cm (292:326)

01-Aug-201211:45:31
TOF MS ES+
5.07e+002

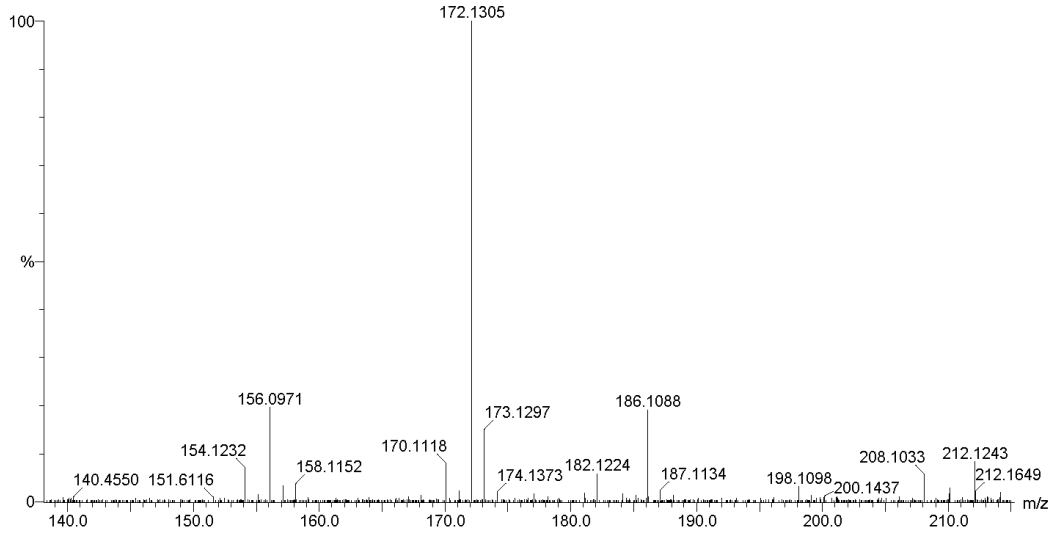

Minimum:				-1.5		
Maximum:		3.0	1000.0	100.0		
Mass	Calc. Mass	mDa	PPM	DBE	i-FIT	Formula
172.1305	172.1338	-3.3	-19.2	1.5	5.6	C9 H18 N O2

Figure 31: HRMS of 1

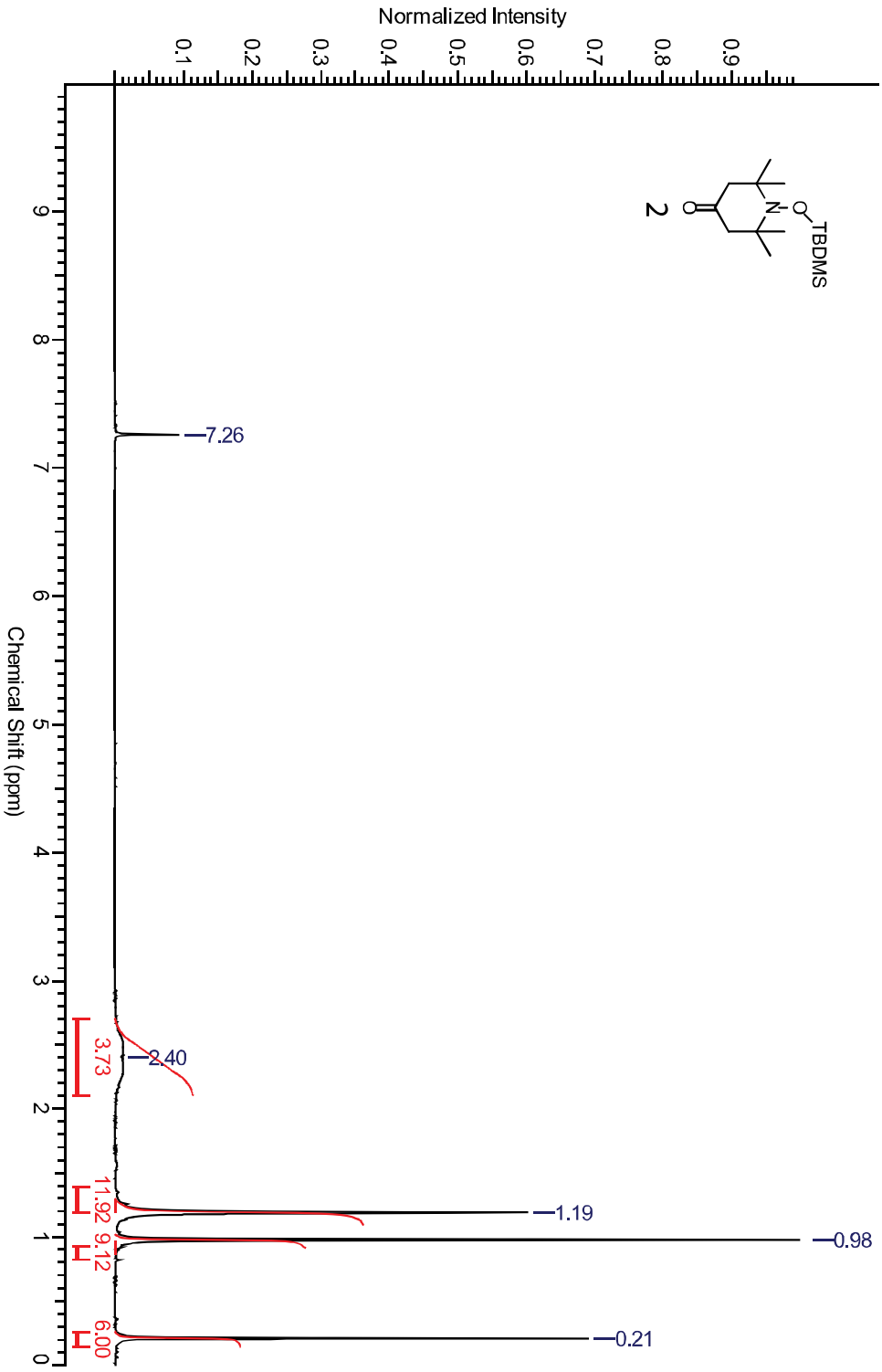

Figure 32: ^{1}HNMR of 2

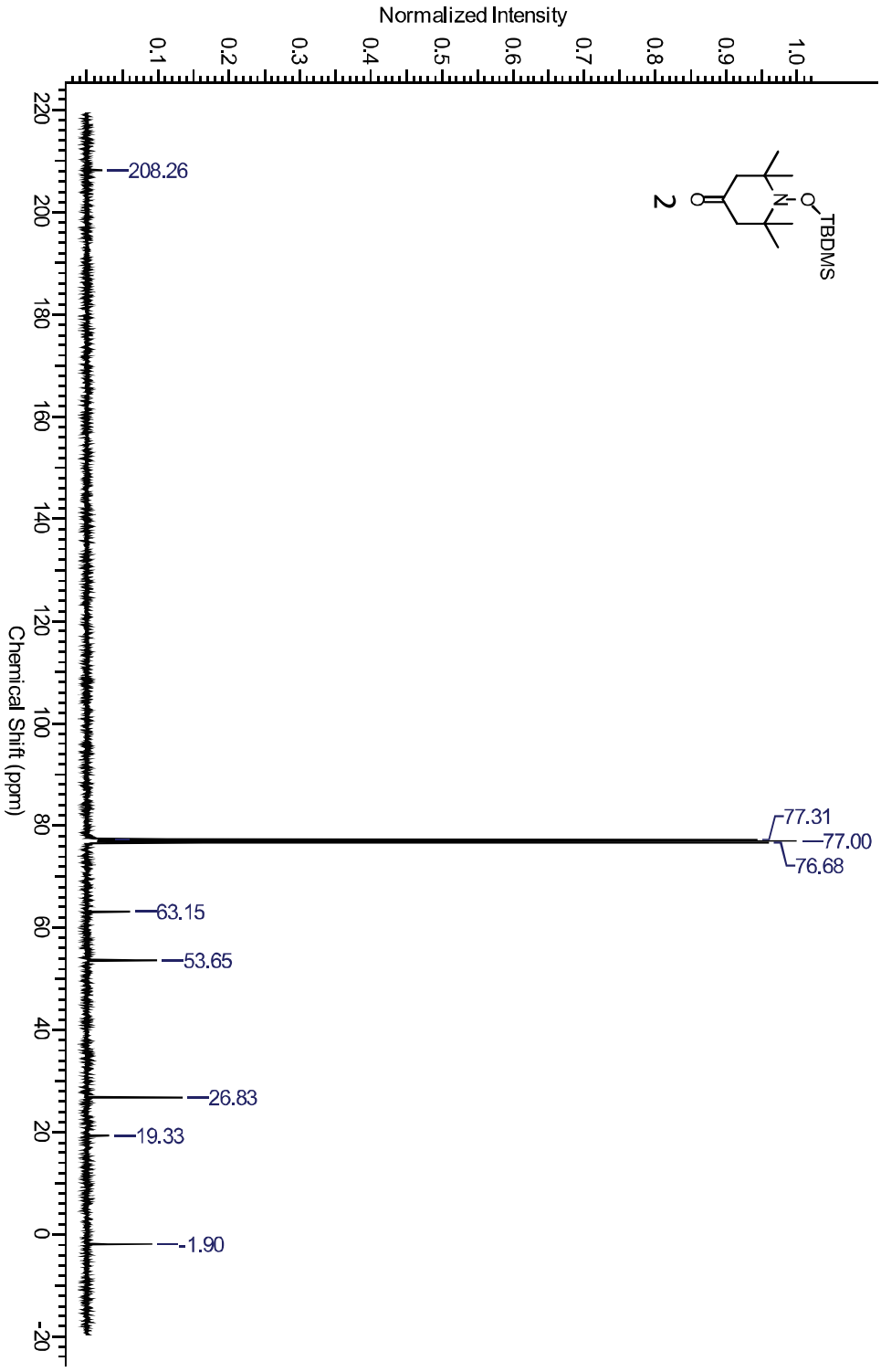

Figure 33: ^{13}CNMR of 2

Elemental Composition Report **Page 1**

Single Mass Analysis
Tolerance = 1000.0 PPM / DBE: min = -1.5, max = 100.0
Element prediction: Off
Number of isotope peaks used for i-FIT = 4

Monoisotopic Mass, Even Electron Ions
12 formula(e) evaluated with 1 results within limits (all results (up to 1000) for each mass)
Elements Used:
C: 0-15 H: 0-32 N: 0-1 O: 0-2 Si: 0-1

MSM-087
69639ASAP 61 (1.153) AM (Cen,3, 80.00, Ar,8000.0,311.08,0.00); Sm (SG, 5x3.00); Cm (61:66)

01-Aug-201210:58:07
TOF MS ES+
1.41e+003

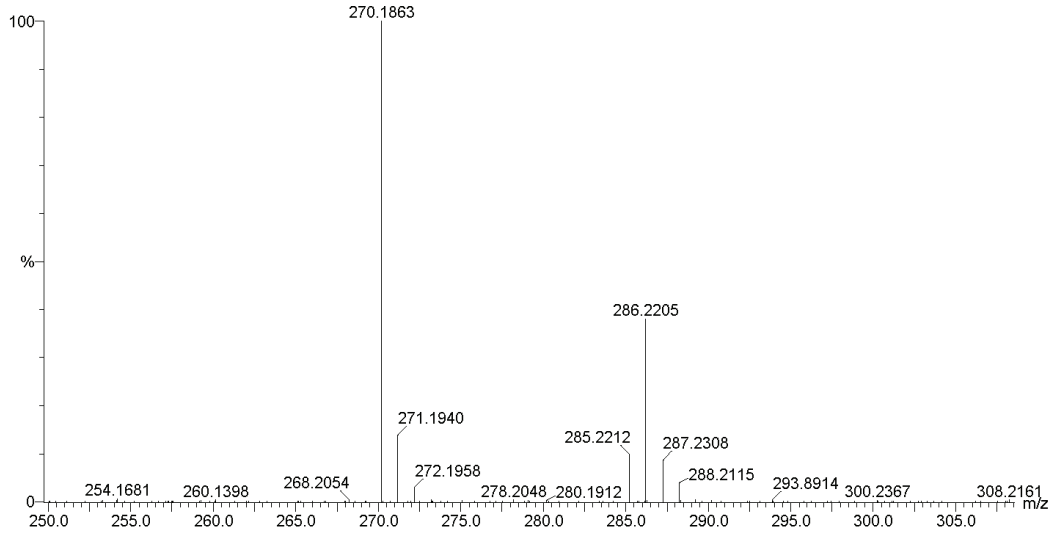

Minimum:				-1.5		
Maximum:		3.0	1000.0	100.0		
Mass	Calc. Mass	mDa	PPM	DBE	i-FIT	Formula
286.2205	286.2202	0.3	1.0	1.5	4.4	C15 H32 N O2 Si

Figure 34: HRMS of 2

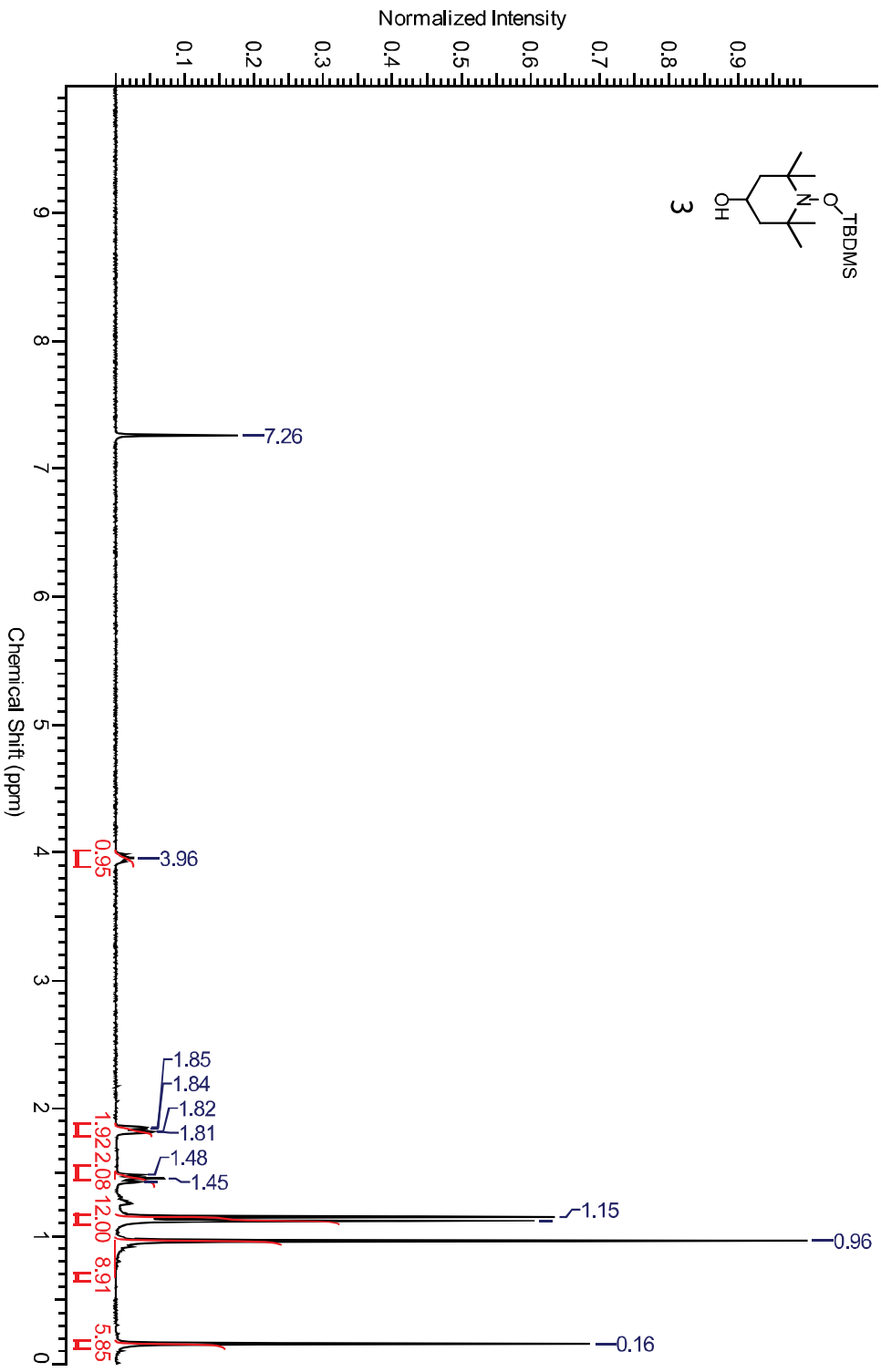

Figure 35: ^{1}HNMR of 3

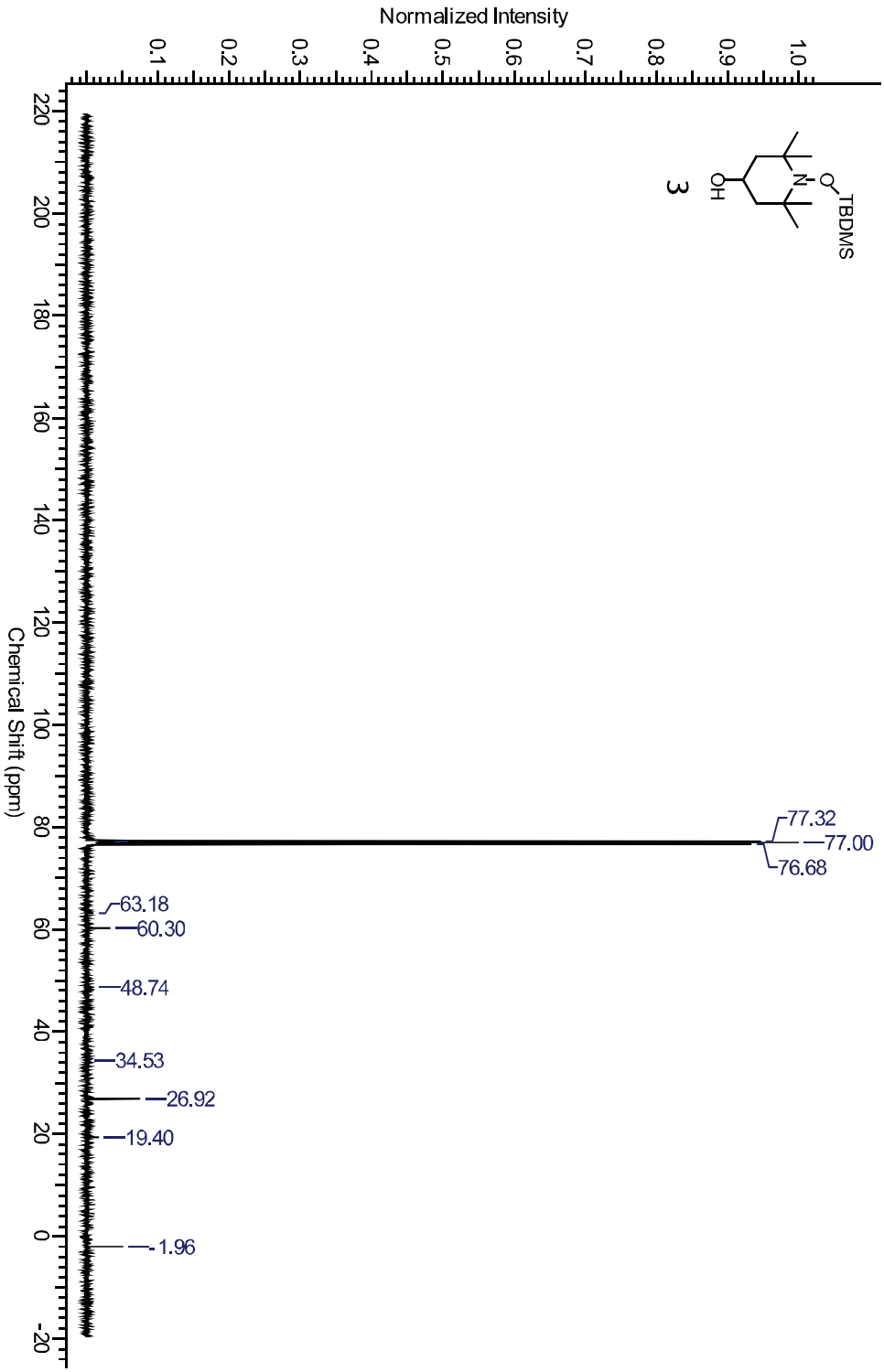

Figure 36: ^{13}CNMR of 3

Elemental Composition Report **Page 1**

Single Mass Analysis
Tolerance = 1000.0 PPM / DBE: min = -1.5, max = 100.0
Element prediction: Off
Number of isotope peaks used for i-FIT = 4

Monoisotopic Mass, Even Electron Ions
12 formula(e) evaluated with 1 results within limits (all results (up to 1000) for each mass)
Elements Used:
C: 0-15 H: 0-34 N: 0-1 O: 0-2 Si: 0-1

MSM-091
69640ASAP 374 (7.033) AM (Cen,3, 80.00, Ar,8000.0,311.08,0.00); Sm (SG, 5x3.00); Cm (340:444)

01-Aug-201211:05:22
TOF MS ES+
4.25e+003

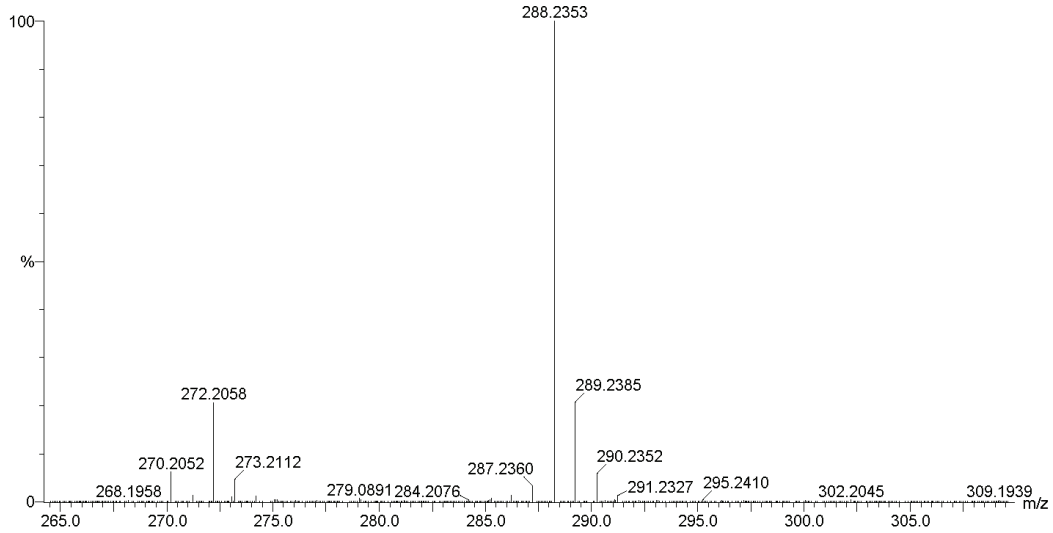

Minimum:				-1.5		
Maximum:		3.0	1000.0	100.0		
Mass	Calc. Mass	mDa	PPM	DBE	i-FIT	Formula
288.2353	288.2359	-0.6	-2.1	0.5	5.8	C15 H34 N O2 Si

Figure 37: HRMS of 3

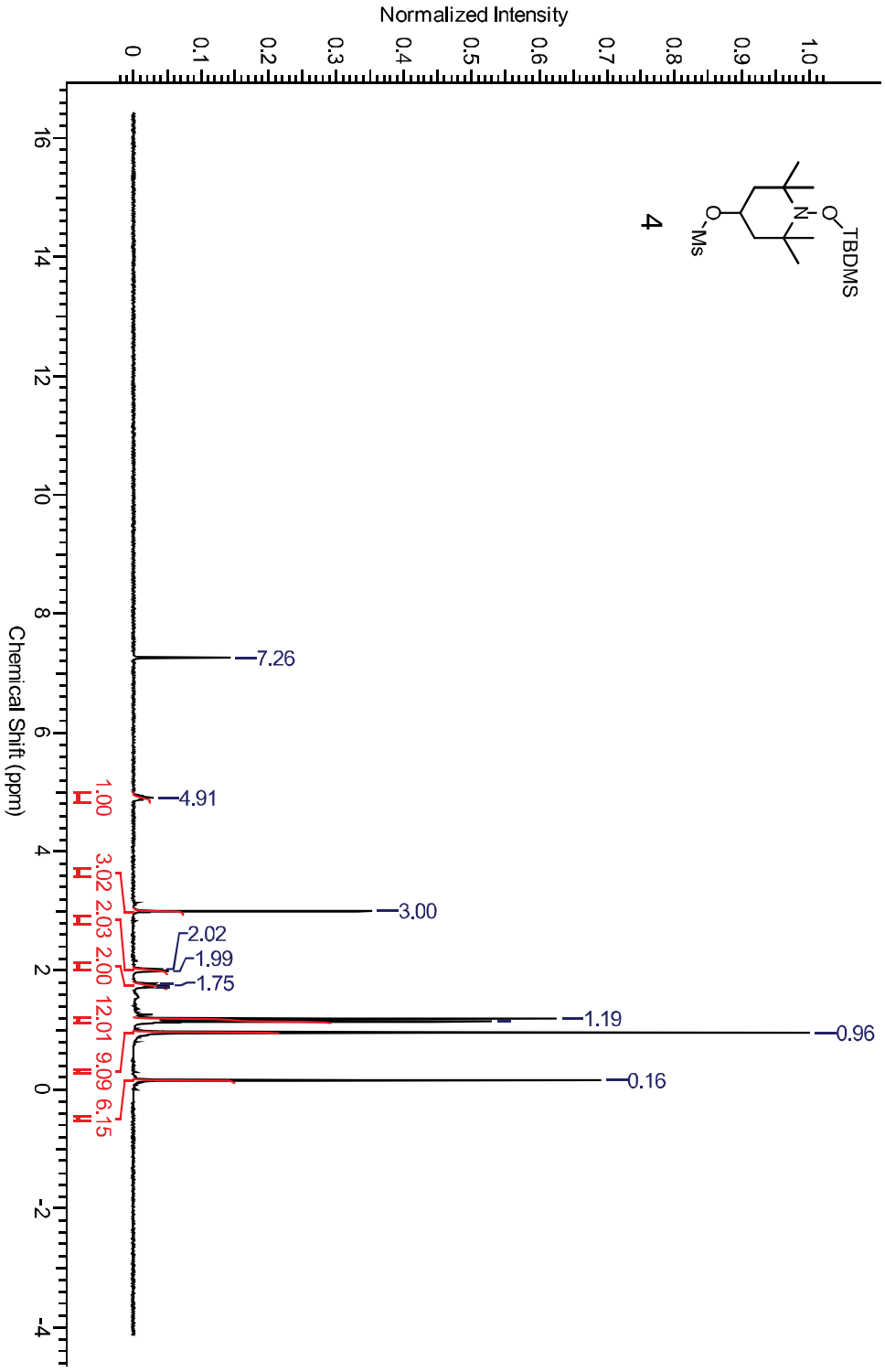

Figure 38: ^{1}HNMR of 4

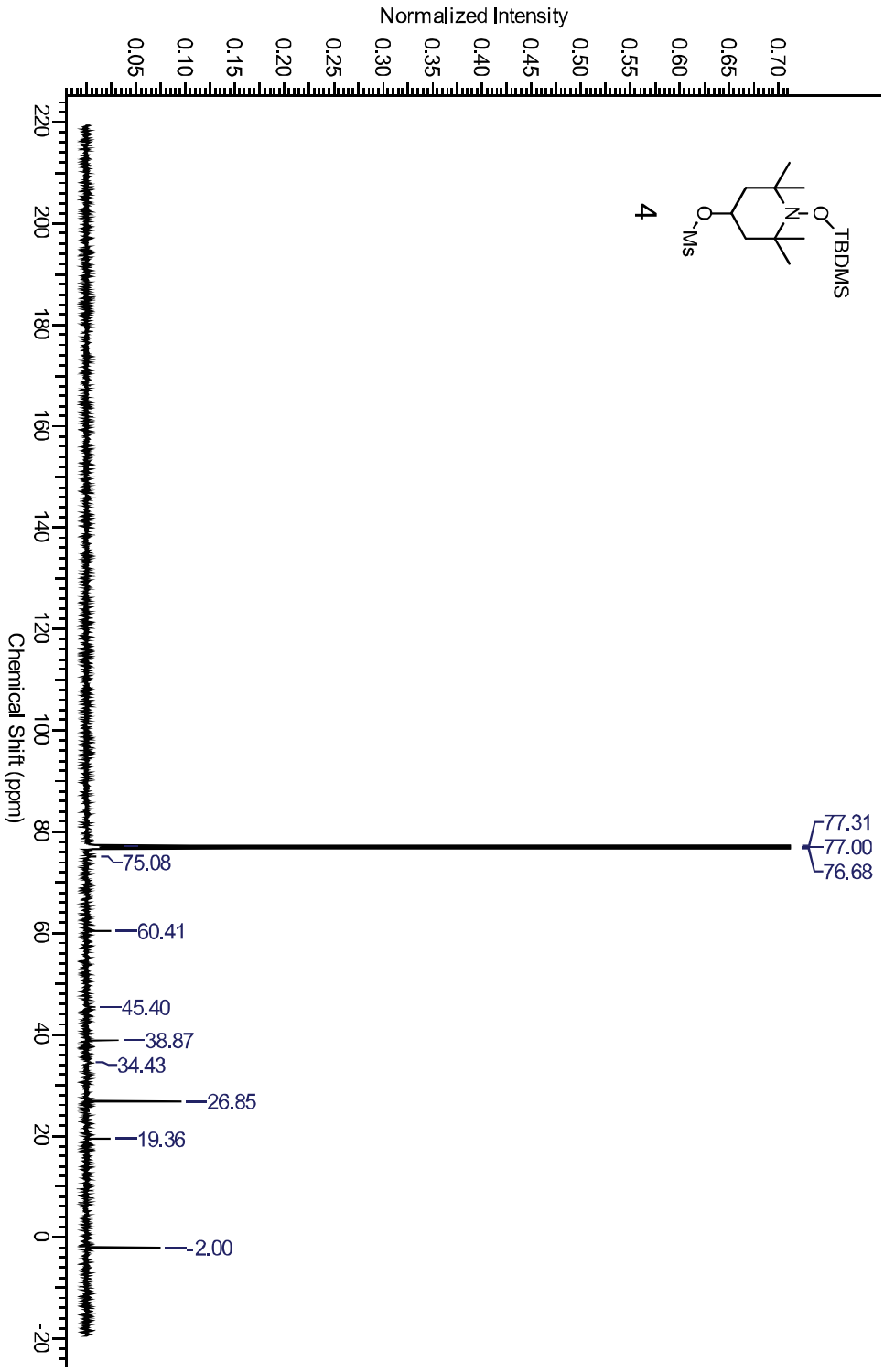

Figure 39: ^{13}CNMR of 4

Elemental Composition Report **Page 1**

Single Mass Analysis
Tolerance = 1000.0 PPM / DBE: min = -1.5, max = 100.0
Element prediction: Off
Number of isotope peaks used for i-FIT = 4

Monoisotopic Mass, Even Electron Ions
40 formula(e) evaluated with 1 results within limits (all results (up to 1000) for each mass)
Elements Used:
C: 0-16 H: 0-36 N: 0-1 O: 0-4 Si: 0-1 S: 0-1

MSM-095
69642ASAP 487 (9.159) AM (Cen,3, 80.00, Ar,8000.0,311.08,0.00); Sm (SG, 5x3.00); Cm (459:489)

01-Aug-201211:54:35
TOF MS ES+
1.20e+004

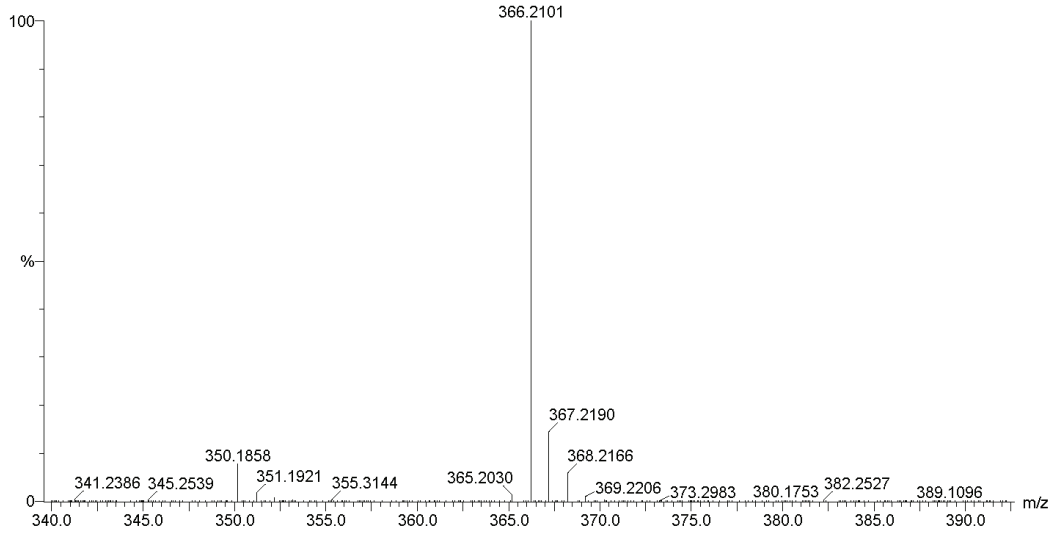

Minimum:				-1.5		
Maximum:		3.0	1000.0	100.0		
Mass	Calc. Mass	mDa	PPM	DBE	i-FIT	Formula
366.2101	366.2134	-3.3	-9.0	0.5	556.3	C16 H36 N O4 Si S

Figure 40: HRMS of 4

BIBLIOGRAPHY

1. *Aboye, T.L., et al., Interlocking disulfides in circular proteins: toward efficient oxidative folding of cyclotides. Antioxid Redox Signal, 2011.* ***14****(1): p. 77-86.*
2. *Gross, A. and W.L. Hubbell, Identification of protein side chains near the membrane-aqueous interface: a site-directed spin labeling study of KcsA. Biochemistry, 2002.* ***41****(4): p. 1123-8.*
3. *Columbus, L. and W.L. Hubbell, A new spin on protein dynamics. Trends Biochem Sci, 2002.* ***27****(6): p. 288-95.*
4. *Barnakov, A., et al., Site-directed spin labeling of a bacterial chemoreceptor reveals a dynamic, loosely packed transmembrane domain. Protein Sci, 2002.* ***11****(6): p. 1472-81.*
5. *Hubbell, W.L., D.S. Cafiso, and C. Altenbach, Identifying conformational changes with site-directed spin labeling. Nat Struct Biol, 2000.* ***7****(9): p. 735-9.*
6. *Hubbell, W.L., et al., Recent advances in site-directed spin labeling of proteins. Curr Opin Struct Biol, 1998.* ***8****(5): p. 649-56.*
7. *Mollaaghababa, R., et al., Time-resolved site-directed spin-labeling studies of bacteriorhodopsin: loop-specific conformational changes in M. Biochemistry, 2000.* ***39****(5): p. 1120-7.*
8. *Battiste, J.L. and G. Wagner, Utilization of site-directed spin labeling and high-resolution heteronuclear nuclear magnetic resonance for global fold determination of large proteins with limited nuclear overhauser effect data. Biochemistry, 2000.* ***39****(18): p. 5355-65.*
9. *Meirovitch, E., et al., Backbone dynamics of deoxy and carbonmonoxy hemoglobin by NMR/SRLS. J Phys Chem B, 2011.* ***115****(1): p. 143-57.*
10. *Tamm, L.K., A.L. Lai, and Y. Li, Combined NMR and EPR spectroscopy to determine structures of viral fusion domains in membranes. Biochim Biophys Acta, 2007.* ***1768****(12): p. 3052-60.*
11. *Chu, S., et al., Solid-state NMR paramagnetic relaxation enhancement immersion depth studies in phospholipid bilayers. J Magn Reson, 2010.* ***207****(1): p. 89-94.*
12. *Bessette, P.H., et al., Efficient folding of proteins with multiple disulfide bonds in the Escherichia coli cytoplasm. Proc Natl Acad Sci U S A, 1999.* ***96****(24): p. 13703-8.*
13. *Wakabayashi, H., A.E. Griffiths, and P.J. Fay, Increasing hydrophobicity or disulfide bridging at the factor VIII A1 and C2 domain interface enhances procofactor stability. J Biol Chem, 2011.* ***286****(29): p. 25748-55.*
14. *Ishizu, K.I., et al., Roles of disulfide linkage and calcium ion-mediated interactions in assembly and disassembly of virus-like particles composed of simian virus 40 VP1 capsid protein. J Virol, 2001.* ***75****(1): p. 61-72.*
15. *Zollner, A., et al., Deletions in the loop surrounding the iron-sulfur cluster of adrenodoxin severely affect the interactions with its native redox partners adrenodoxin reductase and cytochrome P450(scc) (CYP11A1). J Inorg Biochem, 2002.* ***91****(4): p. 644-54.*
16. *Engstrom, L.M., O.A. Partington, and S.S. David, An iron-sulfur cluster loop motif in the Archaeoglobus fulgidus uracil-DNA glycosylase mediates efficient uracil recognition and removal. Biochemistry, 2012.* ***51****(25): p. 5187-97.*
17. *Langen, R., et al., Crystal structures of spin labeled T4 lysozyme mutants: implications for the interpretation of EPR spectra in terms of structure. Biochemistry, 2000.* ***39****(29): p. 8396-405.*
18. *Cunningham, T.F., et al., High-Resolution Structure of a Protein Spin-Label in a Solvent-Exposed beta-Sheet and Comparison with DEER Spectroscopy. Biochemistry, 2012.* ***51****(32): p. 6350-9.*
19. *Nienaber, V.L. and L.J. Berliner, Atomic structures of two nitroxide spin labels complexed with human thrombin: comparison with solution studies. J Protein Chem, 2000.* ***19****(2): p. 129-37.*
20. *Columbus, L., et al., Molecular motion of spin labeled side chains in alpha-helices: analysis by variation of side chain structure. Biochemistry, 2001.* ***40****(13): p. 3828-46.*

21. *Sarver, J.L., et al., Simulating the dynamics and orientations of spin-labeled side chains in a protein-DNA complex. J Phys Chem B, 2012.* ***116****(13): p. 4024-33.*
22. *Fleissner, M.R., D. Cascio, and W.L. Hubbell, Structural origin of weakly ordered nitroxide motion in spin-labeled proteins. Protein Sci, 2009.* ***18****(5): p. 893-908.*
23. *Lietzow, M. and W. Hubbell, Motion of spin label side chains in cellular retinol-binding protein: correlation with structure and nearest-neighbor interactions in an antiparallel beta-sheet. Biochemistry, 2004.* ***43****(11): p. 3137-3151.*
24. *McHaourab, H.S., et al., Motion of spin-labeled side chains in T4 lysozyme. Correlation with protein structure and dynamics. Biochemistry, 1996.* ***35****(24): p. 7692-704.*
25. *Bernardes, G.J., et al., Facile conversion of cysteine and alkyl cysteines to dehydroalanine on protein surfaces: versatile and switchable access to functionalized proteins. J Am Chem Soc, 2008.* ***130****(15): p. 5052-3.*
26. *Chalker, J.M., et al., Methods for converting cysteine to dehydroalanine on peptides and proteins. Chemical Science, 2011.* ***2****(9): p. 1666-1676.*
27. *Schreier, S., et al., The spin label amino acid TOAC and its uses in studies of peptides: chemical, physicochemical, spectroscopic, and conformational aspects. Biophys Rev, 2012.* ***4****(1): p. 45-66.*
28. *van Hest, J.C. and D.A. Tirrell, Efficient introduction of alkene functionality into proteins in vivo. FEBS Lett, 1998.* ***428****(1-2): p. 68-70.*
29. *Ferreira, P.M.T., et al., Michael addition of thiols, carbon nucleophiles and amines to F17 dehydroamino acid and dehydropeptide derivatives. Journal of the Chemical Society-Perkin Transactions 1, 2001(23): p. 3167-3173.*
30. *Yamaguchi, M., et al., A Highly Stereoselective Michael Reaction of Simple Ester Enolates to Alpha,Beta-Unsaturated Esters. Tetrahedron Letters, 1984.* ***25****(49): p. 5661-5664.*
31. *Specht, K.M., et al., Determining absolute configuration in flexible molecules: A case study. Journal of the American Chemical Society, 2001.* ***123****(37): p. 8961-8966.*
32. *Kocherginsky, N. and H.M. Swartz, Nitroxide spin labels : reactions in biology and chemistry. 1995, Boca Raton, Fla.: CRC Press. 270 p.*
33. *Weil, J.A. and J.R. Bolton, Electron paramagnetic resonance : elementary theory and practical applications. 2nd ed. 2007, Hoboken, N.J.: Wiley-Interscience. xxiii, 664 p.*
34. *Hanneke, D., S. Fogwell, and G. Gabrielse, New measurement of the electron magnetic moment and the fine structure constant. Phys Rev Lett, 2008.* ***100****(12): p. 120801.*
35. *Columbus, L. and W. Hubbell, Mapping backbone dynamics in solution with site-directed spin labeling: GCN4-58 bZip free and bound to DNA. Biochemistry, 2004.* ***43****(23): p. 7273-7287.*
36. *David, E.B., et al., Nonlinear-Least-Squares Analysis of Slow-Motion EPR Spectra in One and Two Dimensions Using a Modified Levenberg–Marquardt Algorithm. Journal of Magnetic Resonance, Series A, 1996.* ***120****.*
37. *Columbus, L., et al., Molecular motion of spin labeled side chains in alpha-helices: analysis by variation of side chain structure. Biochemistry, 2001.* ***40****(13): p. 3828-3846.*
38. *Fleissner, M., D. Cascio, and W. Hubbell, Structural origin of weakly ordered nitroxide motion in spin-labeled proteins. Protein science : a publication of the Protein Society, 2009.* ***18****(5): p. 893-908.*
39. *Hahn, E.L., Spin Echoes. Physical Review, 1950.* ***80****(4): p. 580-594.*
40. *Larsen, R.G. and D.J. Singel, Double electron--electron resonance spin--echo modulation: Spectroscopic measurement of electron spin pair separations in orientationally disordered solids. The Journal of Chemical Physics, 1993.* ***98****(7): p. 5134-5146.*
41. *Stryer, L. and R. Haugland, Energy transfer: a spectroscopic ruler. Proceedings of the National Academy of Sciences of the United States of America, 1967.* ***58****(2): p. 719-726.*

42. *Hagen, W., EPR spectroscopy as a probe of metal centres in biological systems. Dalton transactions (Cambridge, England : 2003), 2006(37): p. 4415-4434.*
43. *Jeschke, G., et al., Data analysis procedures for pulse ELDOR measurements of broad distance distributions. Applied Magnetic Resonance, 2004.* ***26****(1): p. 223-244.*
44. *Jeschke, G., et al., DeerAnalysis2006—a comprehensive software package for analyzing pulsed ELDOR data. Applied Magnetic Resonance, 2006.* ***30****(3): p. 473-498.*
45. *Jeschke, G., DEER distance measurements on proteins. Annual review of physical chemistry, 2012.* ***63****: p. 419-446.*
46. *Jeschke, G., et al., Interresidual distance determination by four-pulse double electron-electron resonance in an integral membrane protein: the Na+/proline transporter PutP of Escherichia coli. Biophys J, 2004.* ***86****(4): p. 2551-7.*
47. *Stone, K.M., et al., Electron spin resonance shows common structural features for different classes of EcoRI-DNA complexes. Angew Chem Int Ed Engl, 2008.* ***47****(52): p. 10192-4.*
48. *Reginsson, G. and O. Schiemann, Pulsed electron-electron double resonance: beyond nanometre distance measurements on biomacromolecules. The Biochemical journal, 2011.* ***434****(3): p. 353-363.*
49. *Jeschke, G. and Y. Polyhach, Distance measurements on spin-labelled biomacromolecules by pulsed electron paramagnetic resonance. Physical chemistry chemical physics : PCCP, 2007.* ***9****(16): p. 1895-1910.*
50. *Schiemann, O. and T. Prisner, Long-range distance determinations in biomacromolecules by EPR spectroscopy. Quarterly reviews of biophysics, 2007.* ***40****(1): p. 1-53.*
51. *Byeon, I.-J.L., J. Louis, and A. Gronenborn, A protein contortionist: core mutations of GB1 that induce dimerization and domain swapping. Journal of molecular biology, 2003.* ***333****(1): p. 141-152.*
52. *Schmidt, H., et al., Crystal polymorphism of protein GB1 examined by solid-state NMR spectroscopy and X-ray diffraction. The journal of physical chemistry. B, 2007.* ***111****(51): p. 14362-14369.*
53. *Kirsten Frank, M., et al., Core mutations switch monomeric protein GB1 into an intertwined tetramer. Nature structural biology, 2002.* ***9****(11): p. 877-885.*
54. *Nadaud, P., et al., Long-range structural restraints in spin-labeled proteins probed by solid-state nuclear magnetic resonance spectroscopy. Journal of the American Chemical Society, 2007.* ***129****(24): p. 7502-7503.*
55. *Thoms, S., et al., Dimer formation of a stabilized Gbeta1 variant: a structural and energetic analysis. Journal of molecular biology, 2009.* ***391****(5): p. 918-932.*
56. *Strop, P., A. Marinescu, and S. Mayo, Structure of a protein G helix variant suggests the importance of helix propensity and helix dipole interactions in protein design. Protein science : a publication of the Protein Society, 2000.* ***9****(7): p. 1391-1394.*
57. *Gronenborn, A.M., et al., A novel, highly stable fold of the immunoglobulin binding domain of streptococcal protein G. Science, 1991.* ***253****(5020): p. 657-61.*
58. *Winkler, R., ESIprot: a universal tool for charge state determination and molecular weight calculation of proteins from electrospray ionization mass spectrometry data. Rapid Commun Mass Spectrom, 2010.* ***24****(3): p. 285-94.*
59. *Morrisett, J. and H. Drott, Oxidation of the sulfhydryl and disulfide groups by the nitroxyl radical. The Journal of biological chemistry, 1969.* ***244****(18): p. 5083-5084.*
60. *W. Murray, R. and M. Singh, A convenient high yield synthesis of nitroxides. Tetrahedron Letters, 1988.* ***29****(37): p. 4677-4680.*
61. *Murray, R.W. and M. Singh, Chemistry of Dioxiranes .11. A Convenient High-Yield Synthesis of Nitroxides. Tetrahedron Letters, 1988.* ***29****(37): p. 4677-4680.*

62. *Wallace, W., et al., Use of in situ-generated dimethyldioxirane for inactivation of biological agents. Environmental science & technology, 2005.* ***39****(16): p. 6288-6292.*
63. *Henry Riyad, H. and T.T. Tidwell, Thermolysis of N tetramethylpiperidinyl triphenylacetate: homolytic fragmentation of a TEMPO ester. Journal of physical organic chemistry, 2003.* ***16****(8): p. 559-563.*
64. *Dane, E., et al., Rigid orthogonal bis-TEMPO biradicals with improved solubility for dynamic nuclear polarization. The Journal of organic chemistry, 2012.* ***77****(4): p. 1789-1797.*
65. *Yamada, K.-i., et al., Synthesis of nitroxyl radicals for Overhauser-enhanced magnetic resonance imaging. Archiv der Pharmazie, 2008.* ***341****(9): p. 548-553.*
66. *Fawzi, N., et al., A rigid disulfide-linked nitroxide side chain simplifies the quantitative analysis of PRE data. Journal of biomolecular NMR, 2011.* ***51****(1-2): p. 105-114.*